



Thermal structure of the shallow upper mantle beneath Italy and neighbouring areas: Correlation with magmatic activity and geodynamic significance

Maria Tumanian ^{a,*}, Maria Luce Frezzotti ^b, Angelo Peccerillo ^c, Enrico Brandmayr ^d, Giuliano F. Panza ^{d,e,f}

^a Institute of Geodynamics, J.L. Calderon 19-21, 020032 Bucharest-37, Romania

^b Department of Geosciences, University of Siena, Via Laterina 8, 53100 Siena, Italy

^c Department of Geosciences, University of Perugia, Piazza Università, 06100 Perugia, Italy

^d Department of Geosciences, University of Trieste, Via Weiss 4, 34127 Trieste, Italy

^e The Abdus Salam International Centre for Theoretical Physics, Earth System Physics Section, SAND group, Costiera 11, 34014 Trieste, Italy

^f Institute of Geophysics, China Earthquake Administration, Minzudaxuenuanlu 5, Haidian District, 100081, Beijing, China

ARTICLE INFO

Article history:

Received 30 September 2011

Accepted 18 July 2012

Available online 26 July 2012

Keywords:

Seismic velocity–temperature conversion

Mantle thermal structure

Magmatism

Tyrrhenian Sea area

ABSTRACT

Using an advanced seismic velocity–temperature conversion technique, we infer the temperature and melt distribution in the upper mantle (down to 300 km) beneath Italy and surroundings, starting from absolute S-wave velocity models. The presence of melt, indicated by the seismic reconstruction of the mantle structure in the Tyrrhenian Sea area, requires an extension of the standard conversion procedure to allow for a correction of seismic velocities for the effect of hydrous melt occurrence.

The thermal structure of the upper mantle along four sections crossing the Tyrrhenian basin and the Italian peninsula is investigated. Some characteristics of the obtained thermal structures and melt distributions are well delineated and in accordance with recent models of the evolution of the Tyrrhenian Sea area. The negative thermal anomalies observed in all sections clearly delineate the subduction process of the Adriatic plate (beneath Umbria, Calabria and the Aeolian arc), or the episode of post-continental convergence (beneath Tuscany), or the thermal effect of the remnant of the Adriatic plate (Campania).

Temperature values at Moho seem to be generally correlated with surface heat flow determinations in the Tyrrhenian Sea area and surroundings, although most sectors of the study area (like Tuscan–Tyrrhenian area, Apennines and Adriatic trough) have not yet reached the steady-state thermal regime. The thermal gradients evaluated in the Adria foreland are high in comparison with those of the back-arc area (Tyrrhenian Sea) and could be an effect of the eastward mantle flow beneath Adria lithosphere or a result of the presence of low fraction of melts ≤ 1 wt.%, which cannot rise in compressive regimes, or both.

The melt fraction distribution obtained by the conversion procedure is approximately correlated with the age of the magmatism, the highest abundance occurring in the southern Tyrrhenian Sea, in accordance with widespread active volcanism in this area.

© 2012 Elsevier B.V. All rights reserved.

Contents

1.	Introduction	370
2.	Calculation of mantle temperatures from seismic wave velocities	370
2.1.	The heterogeneous composition of the Italian mantle	370
2.2.	The conversion technique	371
2.2.1.	Anharmonicity	372
2.2.2.	Anelasticity	372
2.2.3.	Melt	373
2.2.4.	Water	373
2.2.5.	Compositional variability	373
2.2.6.	Uncertainties in the thermodynamic parameters	373
2.3.	Sensitivity of temperature of the Vs – T conversion technique	374
3.	Results	375
3.1.	Section 1: Southern Sardinia–Eastern Aeolian Arc–Southern Calabria–Ionian Sea (cells B-2 to B4, C5 to C7, D7)	376
3.2.	Section 2: Northern Sardinia–Southern Apulia (cells A-2 to A8)	376

* Corresponding author. Tel./fax: +40 213172127.

E-mail address: mioara_tumanian@yahoo.com (M. Tumanian).

3.3.	Section 3: Central Tyrrhenian Sea – Latium–Umbria–Marche–Adriatic Sea (cells b0 to b7)	377
3.4.	Section 4: Northern Tyrrhenian Sea – Tuscany–Umbria–Adriatic Sea (cells b-1, b0, c1 to c5)	377
4.	Discussion	377
4.1.	Influence of the assumptions made on mantle composition and water content on the temperature's field	377
4.2.	Temperature models in relation with the heat flow determinations	378
4.3.	Thermal models and their geodynamic significance	378
4.4.	Melt distribution and relation with magmatism	379
5.	Conclusions	379
	Acknowledgments	380
	Appendix A.	380
	Appendix B.	380
	Appendix C.	380
	Appendix D.	380
	References	384

1. Introduction

The direct measurement of temperatures in the Earth's interior is limited to the uppermost crust. The actual temperature estimate in the upper mantle could be, in principle, obtained by extrapolation of the measurements of the surface heat flow. Nevertheless, the heterogeneity of the continental crust reduces our capability of determining realistic temperature values for the lower crust and upper mantle by extrapolation of the near surface temperature measurements. Given the complexity of the temperature field, the temperature determinations (continental geotherms) obtained by surface heat flow extrapolation need to be constrained at great depth by additional data, provided by thermo-barometric or geophysical methods (based on the interpretation of geophysical data and the information coming from experimental studies). The seismic velocities derived from seismic tomography, better absolute models (e.g. <http://www.mantleplumes.org/BananaDoughnuts.html>), together with mineral physics data are frequently used for this purpose (e.g. Sobolev et al., 1996; Goes et al., 2000; Röhm et al., 2000; Kuskov et al., 2006; Tesauro et al., 2009).

The Mediterranean area is one of the most extensively studied regions of the European domain, nevertheless the debate about the geodynamic evolution of this realm is still open. The present geodynamic features of the Western Mediterranean region are the result of eastward migration of the Adriatic–Ionian subduction zone and of the consequent widespread back-arc extension process started about 10–15 Ma ago (Tyrrhenian Sea) (Panza and Calcagnile, 1979; Royden and Burchfiel, 1989; Doglioni, 1991). The seismic models of the upper mantle structure in the Tyrrhenian Sea area indicate the presence of partial melting at shallow depths for the Apennines–Tyrrhenian igneous system (Fig. 1a) and the absence of a plume beneath Italy and the back-arc basin (Peccerillo and Lustrino, 2005; Panza et al., 2007a, 2007b).

The thermal structure of the area, as described by temperature distribution with depth, could contribute to the debate on the geodynamic evolution of the study area. For active volcanic regions, information on temperature distribution in the upper mantle is based mainly on xenoliths geotherms (Artemieva and Mooney, 2001; Artemieva, 2006). The spatial distribution of xenoliths, however, is generally scarce and they represent only the lithospheric upper mantle (Frezzotti et al., 2009 and references therein). Therefore, indirect approaches are needed. Knowledge about the temperature structure of the upper mantle can be improved using the information contained in seismic velocity data. Therefore, despite some uncertainties, a velocity–temperature conversion technique is an alternative source of information about the thermal regime of the upper mantle.

The occurrence of partial melt, pointed out by the interpretation of the seismic tomography in the Tyrrhenian Sea (Panza et al., 2007a, 2007b), prompted us to develop an extension of the standard conversion

technique that includes the sensitivity of the temperature derived from V_s (shear-waves velocity) to the hydrous melt presence. This enhanced procedure provides supplementary information concerning the melt fraction (MF) in the upper mantle, corresponding to the temperature value inferred by the conversion. The degree of melting is modelled as a function of pressure, temperature and weight fraction of water dissolved in the melt.

In this study we use the three dimensional V_s models obtained by the non-linear inversion of surface wave in the Western Mediterranean area by Panza et al. (2007a) and Panza and Raykova (2008), in which the lithosphere–asthenosphere velocity structure is reconstructed to depths of about 300 km for 125 cells, each with size $1^\circ \times 1^\circ$ (Fig. 1b). The obtained 125 representative cellular solutions (cellular models) correspond to the preferred V_s -depth distributions, derived from the nonlinear tomographic inversion, following the optimization procedure described by Boyadzhiev et al. (2008).

2. Calculation of mantle temperatures from seismic wave velocities

2.1. The heterogeneous composition of the Italian mantle

The composition of the upper mantle beneath Italy, inferred from mineralogy of mantle xenoliths occurring at a few localities (Fig. 1b), consists of spinel peridotites (harzburgites and lherzolites, \pm dunites), that may contain variable amounts of hydrous phases, such as phlogopite and amphiboles, and carbonates (Table 1; Conticelli and Peccerillo, 1990; Conticelli, 1998; Jones et al., 2000; Sapienza and Scribano, 2000; Beccaluva et al., 2001a, 2001b; Downes et al., 2002; Frezzotti et al., 2009 and references therein).

In mantle xenoliths from the Tyrrhenian Sea region (i.e. Torre Alfina in Central Italy), relevant and variable amounts of amphibole and phlogopite (up to 10 vol.%) reflect the occurrence of metasomatic events caused by fluids and/or melts rich in water. In subduction zones, the presence of phlogopite may derive from the interaction between slab-released fluids and mantle peridotite (Wyllie and Sekine, 1982; Sassi et al., 1994). The wide (P,T) range of stability of phlogopite in ultramafic compositions suggests its important role in the process of water storage in the upper mantle (e.g. Wendlandt and Egger, 1980; Sudo and Tatsumi, 1990), in the metasomatism occurring above subducting slabs and within mantle wedges, as well as in melting processes (Luth, 1997). Phlogopite can occur both in the lithospheric and asthenospheric mantle, down to its stability limit (200 km). In the Tyrrhenian Sea region variable degrees of metasomatic modifications have been indicated by petrological and geochemical studies of volcanic rocks, with extremely high values beneath the volcanic areas of the Italian peninsula (Peccerillo, 1990, 2005). This suggests high abundance of phlogopite, which may reach locally concentrations as high as 20%, as observed for example in Finero peridotite massif (Zappone, 1994; Zanetti et al., 1999).

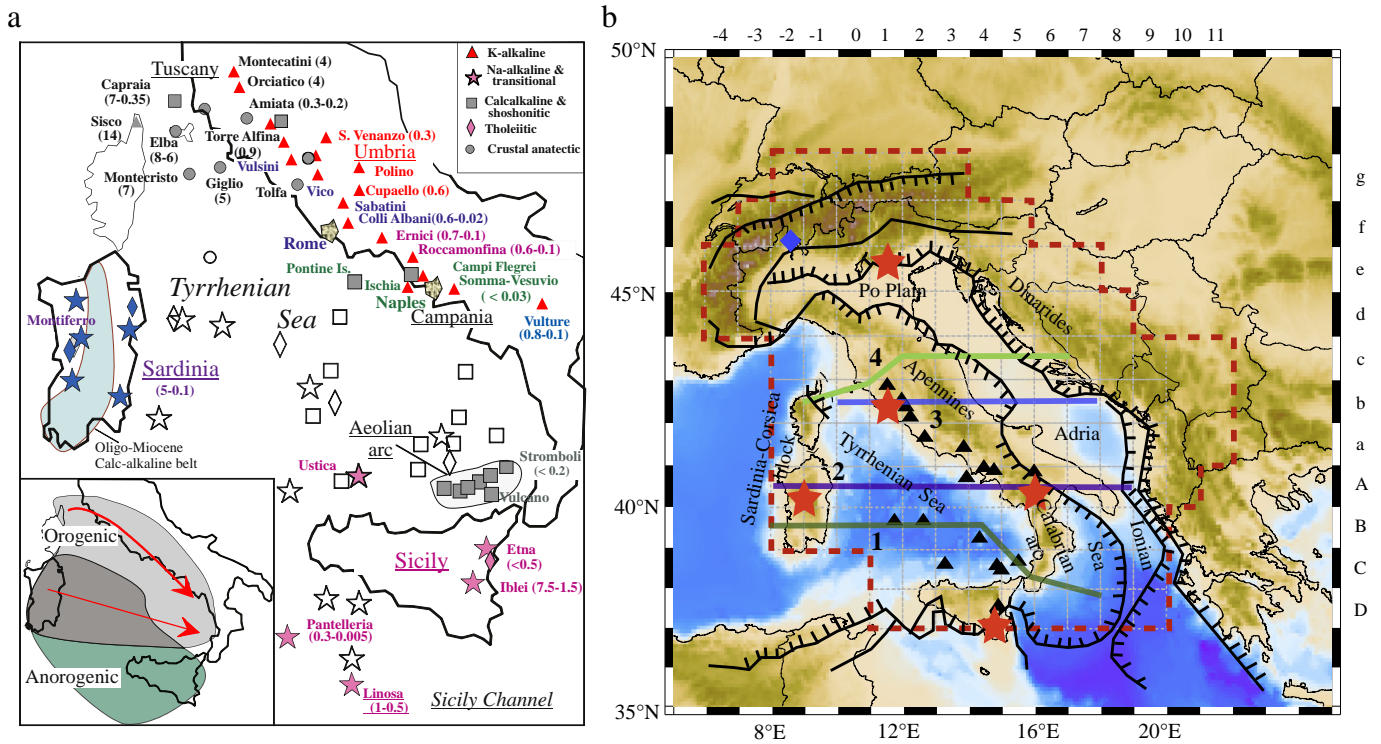


Fig. 1. a) Distribution of Plio-Quaternary magmatism in Italy. Open symbols indicate seamounts. Ages (in Ma) are given in parentheses. Inset: schematic distribution of orogenic and anorogenic volcanism: arrows (red) show migration of orogenic magmatism with time. (Modified after Peccerillo, 2005); b) the study area with cells sized 1×1. Main tectonic lineaments are shown, comb lines indicating compressive fronts and single lines indicating transfer zones. Major volcanoes and seamounts are indicated by triangles, while stars indicate main mantle xenolith localities (see Table 1 for details). Diamond (blue) indicates Finero's peridotite complex. The cell's alphanumeric label is given as well with the location of the cross-sections analysed in this paper, shown by (colour) lines. (For interpretation of the references to colour in this figure legend, the reader is referred to the web version of this article.)

To account for the complexity of the upper mantle composition beneath the Tyrrhenian Sea region, the two compositions, variable with depth, shown in Table 2, have been adopted in this study. The first is from the Finero peridotite massif (Western Alps, Fig. 1b) (Hartmann and Wedepohl, 1993), one of the best examples of metamorphic phlogopite peridotite massif emplaced during Variscan orogeny in Italy. The second is from peridotitic xenoliths (Authors' unpublished data, Table 1) included within the Torre Alfina ultrapotassic rocks from Tuscany (Central Italy; Fig. 1a and b). These compositional models take into account the solid–solid phase transition in the mantle peridotites from spinel to garnet.

The compositional complexity of the upper mantle in the foreland areas in Mediterranean region, in terms of the volumetric proportion λ ,

assuming the mantle rock compositions reported in Table 1, is represented by the three reference compositional models defined in Table 3.

2.2. The conversion technique

The characteristics of the seismic wave propagation are strongly controlled by the thermal and mechanical properties of the sampled rocks. The relationship between temperature, composition and seismic velocity has been largely investigated (Furlong et al., 1995; Sobolev et al., 1996; Goes et al., 2000; Röhm et al., 2000). The effect of temperature on seismic wave velocity and elastic parameters of rocks samples has been proved in laboratory experiments, as reported in the pioneering paper by Birch (1943) and more recently

Table 1
Average modal mineral compositions (vol. %) for the Italian mantle xenolith rocks.

Location	Rock	OI vol. %	Mg#	Opx vol. %	Mg#	Cpx vol. %	Sp vol. %	Amph vol. %	Phl vol. %	Temperature °C	Pressure GPa	References
Torre Alfina (Central Italy)	Harzburgite	80–95	0.90–0.92	4–12	0.91–0.93	<1–8	1–2	0	<1–10	950–1080	1.6 ± 0.2	1, 2, 3, 4
	Dunite											
Vulture (Southern Italy)	Lherzolite	60–86	0.90–0.91	8–30	0.91–0.93	1–10	1–2	1	Traces	992–1150	1.8 ± 0.3	5, 6, 7
	Harzburgite											
Sardinia	Lherzolite	60–80	0.89–0.91	10–30	0.90–0.92	4–16	1–3	0	0	950–1050	1.4 ± 0.2	1, 8
	Harzburgite											
Iblei (Sicily)	Harzburgite	60–77	0.90–0.92	10–30	0.87–0.91	3–10	1–4	Traces	Traces	950–1050	1	1, 9, 10
	Lherzolite											
VVP (Northern Italy)	Lherzolite	45–70	0.89–0.91	20–40	0.89–0.91	3–15	2–8	Traces	0	750–980, 1280–1370	1.7 ± 0.3	1, 11, 12, 13
	Harzburgite											

OI = olivine; Opx = orthopyroxene; Cpx = clinopyroxene; Sp = spinel; Amph = amphibole; Phl = phlogopite; Mg# = Mg/(Mg/Fetot); VVP = Veneto Volcanic Province; 1 authors' unpublished data; 2 Conticelli and Peccerillo, 1990; 3 Conticelli, 1998; 4 Pera et al., 2003; 5 Jones et al., 2000; 6 Downes et al., 2002; 7 Rosatelli et al., 2007; 8 Beccaluva et al., 2001a; 9 Sapienza and Scribano, 2000; 10 Sapienza et al., 2005; 11 Morten and Bondi, 1981; 12 Siena and Coltorti, 1989; 13 Beccaluva et al., 2001b.

Table 2

Assumed compositions for the Tyrrhenian Sea back-arc area and their variations with depth.

Minerals (λ_i)(%)	Depth range (km)	OI	Opx	Cpx	Gt	Sp	Amph	Phl
Finero composition	Moho–80 km	74	16	3	0	1	5	1
	81–200 km	74	16	3	1	0	0	6
	201–300 km	78	18	3	1	0	0	0
Torre Alfina composition	Moho–80 km	83	8	5	0	2	0	2
	81–200 km	83	8	5	2	0	0	2
	201–300 km	85	8	5	2	0	0	0

by Jackson et al. (1992) and Jackson (2000). A number of studies (Sobolev et al., 1996; Artemieva and Mooney, 2001; Artemieva et al., 2004) confirm the hypothesis that compositional variations in the upper mantle, indicated by xenoliths, are of minor importance when compared to the effect of temperature on the seismic wave velocities.

The seismic velocity–temperature relationship is strongly nonlinear and it is influenced by several perturbing factors, such as the variable mantle composition, the presence of melt material and of fluids in the upper mantle, the anelastic behaviour of the propagation medium at the high temperatures in the mantle (Karato, 1993; Tsumura et al., 2000; Nakajima and Hasegawa, 2003; Priestley and McKenzie, 2006). Here we develop an extension of the seismic velocity–temperature conversion method formulated by Goes et al. (2000) for the shallow mantle, in which the effect of compositional variations and corrections for the effect of anelasticity, and for the melt and water presence in the mantle rocks, are considered.

2.2.1. Anharmonicity

In a symmetric or parabolic potential well, the mean positions of atoms are unchanged, atomic vibrations are harmonic and no thermal expansion results. In nature, the thermal oscillation of atoms in their (asymmetric) potential well is anharmonic or nonsinusoidal; thermal oscillation of an atom causes the mean position to be displaced, and thermal expansion results (Anderson, 2007). For each mineral composing the upper mantle rocks, the elastic (anharmonic) parameters (shear modulus, μ ; bulk modulus, K) and density (ρ) are calculated as a function of temperature (T), pressure (P) and iron content (X) applying the standard relations of infinitesimal strain theory used by Goes et al. (2000) and Shapiro and Ritzwoller (2004).

The upper mantle is assumed to be composed of three main minerals (olivine, orthopyroxene, clinopyroxene), plus minor garnet/spinel and accessory phlogopite and amphiboles (Tables 2 and 3).

For the first five minerals most of the values of density and elastic parameters and of their derivatives $\frac{\partial \rho}{\partial X}, \frac{\partial K}{\partial X}, \frac{\partial \mu}{\partial X}, \frac{\partial K}{\partial T}, \frac{\partial \mu}{\partial T}, \frac{\partial K}{\partial P}, \frac{\partial \mu}{\partial P}$, determined through laboratory experiments, have been taken from Goes et al. (2000) and Cammarano et al. (2003). For phlogopite and amphiboles the values of the thermo-elastic parameters $\rho, K, \mu, \alpha_0, \frac{\partial K}{\partial P}, \frac{\partial \mu}{\partial P}$ are constrained with information from literature (Anderson and Isaak, 1995; Hacker et al., 2003; Pavese et al., 2003; Kopylova et al., 2004; Anderson, 2007; Ji et al., 2009). Here, α_0 is the coefficient of the thermal expansion at temperature $T_0 = 0^\circ\text{C}$. Due to the scarcity of

Table 3

Reference compositional models of the upper mantle of the foreland area (Adriatic–Ionian domain). For cell location see Fig. 1b.

Minerals (λ_i)(%)	OI	Opx	Cpx	Gt	Sp	Amph	Phl
For cells b5–b7; c5	85	8	5	0	2	0	0
A7–A8	70	18	10	0	2	0	0
C7; D7	70	20	7	0	3	0	0

literature information about the other physical parameters of phlogopite and amphiboles, the following assumptions are made:

- (1) the values assigned to $\frac{\partial \rho}{\partial X}, \frac{\partial K}{\partial X}, \frac{\partial \mu}{\partial X}$ are similar to those given by Cammarano et al. (2003) for two other hydrous phases (hydrous wadsleyite and ringwoodite);
- (2) based on Anderson (1988) observation that the values of $\frac{\partial K}{\partial T}, \frac{\partial \mu}{\partial T}$ are remarkably constant for a wide variety of materials, the mean values determined for silicates are assigned to phlogopite and amphiboles as well;
- (3) the values for the thermal expansion coefficients $\alpha_1, \alpha_2, \alpha_3$ for the hydrous phase A (Phan, 2008) are assigned to phlogopite and amphiboles. Phase A, $\text{Mg}_7\text{Si}_2\text{O}_8(\text{OH})_6$, is a dense hydrous magnesium silicate obtained in high-pressure experiments, that could store and transport the water into the Earth's mantle and the subduction zones. All the values adopted for the parameters mentioned in this section are given in Appendix A (Table A.1).

In the conversion procedure the variability of mantle composition has been taken into account and it is evaluated through average physical parameters for a given composition, as a function of the volumetric proportion of each individual mineral λ_i (Tables 2 and 3), using the Voight–Reuss–Hill (VRH) averaging scheme (Appendix B).

2.2.2. Anelasticity

The anelastic behaviour of the material composing the upper mantle manifests itself through seismic waves amplitude attenuation and it is often evaluated using the quality factor of the medium, Q_s (for shear waves). Following the attenuation model proposed by Minster and Anderson (1981), the quality factor is given by:

$$Q_s(P, T, \omega) = A\omega^3 \exp\left[\frac{H^* + PV^*}{RT}\right] \quad (1)$$

where A and a are constants, H^* is the activation energy, V^* is the activation volume domain, ω is the seismic waves angular frequency, P is the pressure, T is the temperature and R is the ideal gas constant ($R = 8.314472 \text{ J}/(\text{mol K})$). To evaluate the correction for attenuation of the seismic waves, we adopt the values proposed by Shapiro and Ritzwoller (2004): $A = 0.045$; $a = 0.15$; $H^* = 500 \text{ kJ mol}^{-1}$; $V^* = 2.0 \cdot 10^{-5} \text{ m}^3 \text{ mol}^{-1}$; $\omega = 2\pi\nu$; $\nu = 1 \text{ Hz}$.

In the conversion procedure the anelastic behaviour of the propagation medium is taken into account as a correction applied to the V_s calculation (Minster and Anderson, 1981):

$$V_{\text{Scor}}(P, T, \omega) = V_s(P, T, \omega) \left[1 - \frac{Q_s^{-1}(P, T, \omega)}{2 \tan(\pi a/2)} \right] \quad (2)$$

Even if Cammarano et al. (2003) indicate that the seismic velocities are not strongly sensitive to variations in Q_s , Q values, to be reliable, must be measured with great care (Levshin et al., 2010). A variation of 50% of Q_s produces a decrease of V_s by about 0.3%, a variation that is comparable with the resolution of our data set. However, if the anelasticity effect is ignored in the conversion technique (Q_s is assumed infinite), important errors in temperature estimates could be introduced.

Following Sobolev et al. (1996) and Goes et al. (2000) the temperature corresponding to the observed seismic velocity $V_{s \text{ ref}}$ (seismic velocity obtained through seismic tomography) is determined using an iterative method:

$$T^{n+1} = T^n + F \left\{ \left[V_{s \text{ ref}} - V_{\text{Scor}}(T^n) \right] / \left[\left(\partial V_s / \partial T \right)_{\text{cor}}(T^n) \right] \right\} \quad (3)$$

with $\left(\frac{\partial V_s}{\partial T} \right)_{\text{cor}} = \left(\frac{\partial V_s}{\partial T} \right)_{\text{anh}} + \left(\frac{\partial V_s}{\partial T} \right)_{\text{anel}}$ and where n represents the iteration number, F is a convergence factor and $V_{s \text{ cor}}$ is the velocity

defined in eq. (2). $\left(\frac{\partial V_s}{\partial T}\right)_{\text{anh}}$ is obtained using the VRH averaging scheme (Appendix B) and $\left(\frac{\partial V_s}{\partial T}\right)_{\text{anel}}$ is expressed as:

$$\left(\frac{\partial V_s}{\partial T}\right)_{\text{anel}} = Q_s^{-1} \frac{aH^*}{2RT^2 \tan(\pi a/2)} \quad (4)$$

The starting temperature T^1 is evaluated with the 1-D thermal model, as a steady-state solution of the 1-D conductive equation with boundary conditions (average value of the surface heat flux and of surface temperature for each study area) and a priori information on the distribution of thermal parameters (thermal conductivity and heat production in the crust) taken from literature (details on the 1-D thermal model are given in Appendix C). When such a procedure is followed, the final temperature is not sensitive to the starting temperature.

2.2.3. Melt

The reconstruction of the elastic mantle structure in the Tyrrhenian Sea area suggests the occurrence of melts at shallow depths (Panza et al., 2007a, 2007b). These findings make it necessary to an extension of the standard conversion procedure: the introduction of a correction of seismic velocities for the effect of melt presence. This aspect has been studied (Schmeling, 1985; Sato et al., 1989) but it is not well constrained by experimental and theoretical results (Goes et al., 2000).

The sensitivity of the seismic velocity to the presence of melt is expressed by a factor named (hereinafter) DVC (the derivative of V_s with respect to the melt content). Values of DVC, taken from literature (Goes et al., 2000), range from 0.7% to 8.5%. This variability, of about one order of magnitude, is due to a manner in which different melt pockets are/are not interconnected (melt geometry) (Mavko, 1980) and signifies that, for an increase of melt quantity by 1%, V_s decreases by 0.7% to 8.5%, a variation that is much larger than the resolution of our data set. For dry peridotite, using the model of McKenzie and Bickle (1988), the enhanced conversion procedure provides supplementary information concerning the melt fraction (MF) in the mantle rocks, corresponding to the temperature value inferred by the conversion. At each iteration step (starting with the first step), a check is made whether the calculated temperature T^n at a given depth is higher than the temperature that corresponds to the solidus curve at the corresponding pressure. If T^n is higher than the solidus (which means that the material at that depth may contain melt), a correction for the presence of melt in the mantle is applied that decreases the anelastic seismic velocity proportionally to the product of DVC by MF. Thus expression (2) is replaced by:

$$V_{\text{cor}}(P, T, \omega) = V_s(P, T, \omega) \left[1 - \frac{Q_s^{-1}(P, T, \omega)}{2 \tan(\pi a/2)} (1 - \text{DVC} * \text{MF}) \right] \quad (5)$$

where MF is calculated following the procedure described by McKenzie and Bickle (1988).

2.2.4. Water

The presence of water in the mantle rocks affects the seismic velocities as well (e.g. Karato and Jung, 1998). One of the principal goals of this study is to determine the effect of H_2O on the partial melting of the mantle. Addition of water to a peridotite system, such as in zones affected by subduction processes, lowers the solidus and increases the degree of melting, in proportion to the dissolved water fraction (Asimow and Langmuir, 2003; Katz et al., 2003; Aubaud et al., 2004; Hirschmann et al., 2009). Therefore, a correction for the presence of hydrous mantle melts has been included in the conversion technique, using the parameterization for hydrous

melting developed by Katz et al. (2003). This parameterization is a quantitative model that reproduces well the experimental database, which includes results predicted by thermodynamic modelling and has the advantage to offer an easy way to be incorporated into an existing algorithm (like velocity–temperature conversion procedure). Katz et al. (2003) performed the calibration of the nominally anhydrous and hydrous models on a set of various rock types. Similar to Asimow and Langmuir (2003), the water is treated as an incompatible element, incorporated in the solid mantle phases. The degree of melting of peridotite under nominally anhydrous and hydrous conditions is modelled as a function of both temperature, and of bulk H_2O content (wt.%). For a peridotite with a given H_2O content, the melt fraction–temperature trend migrates to progressively lower temperatures relative to the nominally anhydrous mantle trend, because of the strong partitioning of H_2O in the partial melt.

Thus, an essential constrain for mantle melting modelling is water-storage capacity of the Italian upper mantle rocks, defined as the maximum H_2O concentration that a peridotite can store without stabilizing hydrous fluids. For the back-arc region, where phlogopite controls the water-storage capacity of peridotites down to a depth of about 200 km, we estimate 0.45 wt.% bulk water content, corresponding to hydrous mantle without excess water (Kelley et al., 2006; Green et al., 2010). At greater depths down to 300 km, where phlogopite is unstable, water-storage capacity as hydroxyls in nominally anhydrous minerals (NAMs) is considerably lower, and we estimate bulk water contents variable from 0.1 to 0.01 wt.% (Bolfan-Casanova, 2005; Hirschmann et al., 2005; Hauri et al., 2006).

For the nominally anhydrous mantle beneath the foreland region, we adopt comparatively small H_2O contents, from 0.1 to 0.01 wt.%. Although it has been shown that the water-storage capacity in NAMs increases with increasing pressure in the considered pressure interval (e.g. Hauri et al., 2006), water content has been assumed homogeneous throughout the foreland mantle sections.

2.2.5. Compositional variability

The sensitivity to temperature of seismic velocities decreases with increasing depth, whereas the influence of variations in composition gains importance (Cammarano et al., 2003). The effects of temperature and composition on seismic velocities are difficult to separate (Kuskov et al., 2006). The upper mantle cannot be treated as uniform in terms of composition, and, consequently, modelling of the cratonic upper mantle by Kuskov et al. (2006) included a continuous change in composition with depth (by a thermodynamic approach), in order to get realistic temperature profiles. To avoid negative thermal gradients inferred from seismic data just below 250 km, Cammarano et al. (2009) invoked a plausible enrichment in the basaltic component with depth. However, Kuskov et al. (2006) suggest that non-physical temperature behaviour could be explained by seismic uncertainties associated with high velocity gradients in the IASP91 model at depths of 210–300 km. To overcome this problem, common to all relative tomography models, absolute velocity models rather than velocity perturbations have to be used in temperature estimates (Goes et al., 2000; Röhm et al., 2000; Cammarano and Romanowicz, 2007). In our study based upon absolute velocity cellular models (Panza et al., 2007a; Panza and Raykova, 2008) the complexity of the upper mantle composition beneath Tyrrhenian Sea region has been taken into account assuming horizontal and vertical variations in the composition of the upper mantle rocks (details are given in Section 2.1).

2.2.6. Uncertainties in the thermodynamic parameters

Thermodynamic (elastic) and anelastic properties of minerals are important parameters controlling density and seismic velocities of mantle rocks. The uncertainties concerning the realistic estimation of thermodynamic parameter values, including errors in calculated bulk properties of the rocks under high pressure and temperature and partial knowledge of composition of the multiphase assemblages

(rocks), are difficult to be evaluated. Therefore, the interpretation of the temperatures derived from V_p (compressional-waves velocity) and V_s measurements is hampered by a number of uncertainties. In the upper mantle above 400 km of depth, the uncertainties in the elastic and anelastic properties of mantle minerals translate into an error in the temperatures inferred from seismic velocities of about ± 100 °C (Cammarano et al., 2003).

2.3. Sensitivity of temperature of the $V_s - T$ conversion technique

In this section we consider the influence on temperature evaluations of the assumptions made on the values of the input parameters used in the velocity to temperature conversion.

The sensitivity of the temperature, derived from V_s , to the presence of melt has been tested for the model displayed in Fig. 2a, using three different DVC values. This velocity model represents, down to a depth of 250 km, the mean seismic structure for cell A7, located in the foreland of Southern Apennines, (see Fig. 1b). A 20 km thick crust overlies a thin mantle wedge, a soft mantle lid following Brandmayr et al. (2010) terminology; a lithospheric mantle (LID), with V_s of 4.55 km/s, extends from 40 to 90 km depth and lies on an asthenospheric layer (LVZ with V_s of 4.45 km/s and 4.6 km/s) which extends down to about 250 km of depth (Panza et al., 2007a).

For cell A7, the composition (shown in Table 3) is assumed constant with depth. In the depth interval from the Moho discontinuity to about 300 km the temperatures derived from V_s are calculated by the enhanced conversion technique described in Section 2.2 and one temperature value at the middle of each layer is plotted in Fig. 2b. On the right panel, the melt fraction distribution in the upper mantle, evaluated by the same enhanced conversion procedure is shown (Fig. 2c).

The result of our parametric tests, shown in Fig. 2, indicates that while there is little effect on the inferred temperature, the melt fraction is strongly influenced by DVC values. Thus, an increase of the V_s sensitivity to the presence of melt by approximately 6 and 11 times leads to a decrease of the melt fraction by about 5 and 9 times, respectively. This result is not surprising since the applied correction for the presence of melt is introduced in such a way to decrease the anelastic seismic velocity by an amount proportional to the product of DVC by MF.

The results of the modelling of water content influence are shown in Fig. 3. The geotherms displayed in Fig. 3b are obtained by the enhanced conversion technique, which includes a correction for the melt fraction evaluated following the model of McKenzie and Bickle (1988) (anhydrous case – dotted line (black)) and the model of Katz et al. (2003) (anhydrous case – thin solid line (red)); hydrous cases – dashed line (cyan), long - dashed line (green), dash - dotted line (magenta), thick solid line (blue) – for different weight fractions of bulk water content). The corresponding profiles of melt fraction are shown in Fig. 3c.

DVC has the same value (DVC=4) in all analysed cases. The results obtained for cell A7 indicate that large water content (0.45 wt.%), in the mantle rocks lowers the calculated temperature values by 12–22%, and increases the melt fraction values by more than 47%. Smaller water content (0.1 wt.%) in the mantle rocks reduces the calculated temperature values by around 9% and increases the melt fraction values by more than 26%. In the anhydrous case, parameterizations developed by McKenzie and Bickle (1988) and Katz et al. (2003) give similar results about the inferred temperatures and melt fractions.

To account for the influence of compositional variability on the inferred temperatures three different compositions have been adopted in the parametric tests. The temperatures for cell a2, located in the Roman Province, are obtained with a mantle composition constant with depth, without hydrous phases (shown in the Table 3, first row) and with the two variable mantle compositions given in Table 2. The last two differ, among others, in the amounts of hydrous phases (phlogopite and amphiboles). The stratified structure of cell a2 is shown in Fig. 4a: the crust, about 25 km thick, lies on a thin hot mantle layer (V_s about 3.9 km/s) that reaches the depth of about 38 km; a fast LID (V_s about 4.6 km/s) extends down to about 50 km of depth; below, the asthenosphere, whose top is marked by a LVZ (V_s about 4.1 km/s and 4.4 km/s) seems to extend to depths as large as 300 km (Panza et al., 2007a).

The thermal results obtained for cell a2 for the three different compositions are displayed in Fig. 4, along with the geotherms obtained by the velocity–temperature conversion procedure (Fig. 4b) and the corresponding profiles of melt fraction (Fig. 4c), using the parameterization developed by Katz et al. (2003). In the modelling, the weight fractions of bulk water content have the same value of 0.45 wt.% and remain constant with depth. The results illustrate a clear tendency in

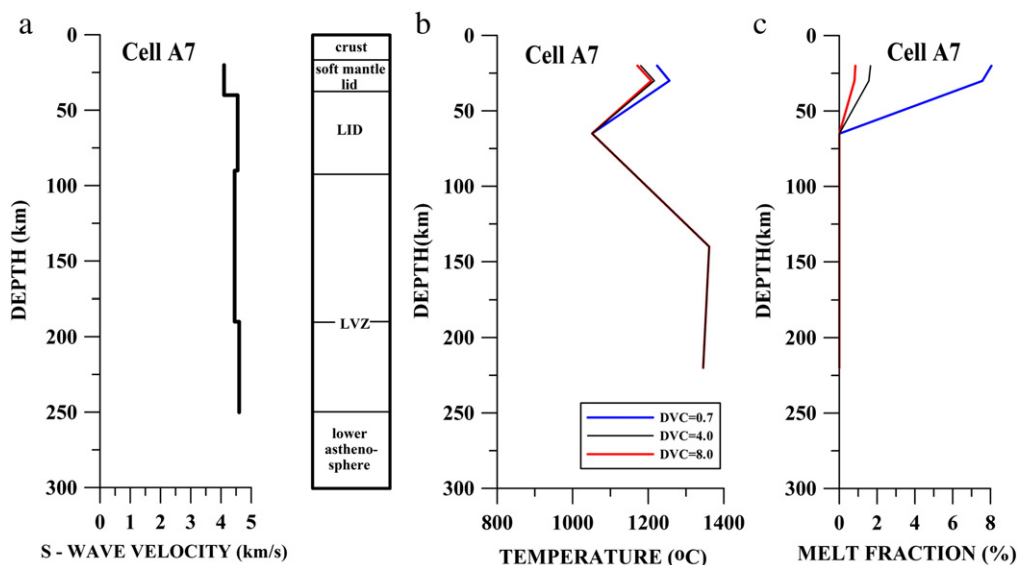


Fig. 2. V_s model of cell A7 (a); sensitivity of temperature (b) and of melt fraction (c) to variation of DVC values. Here and in the following figures LVZ marks the bottom of the low velocity zone in the asthenosphere.

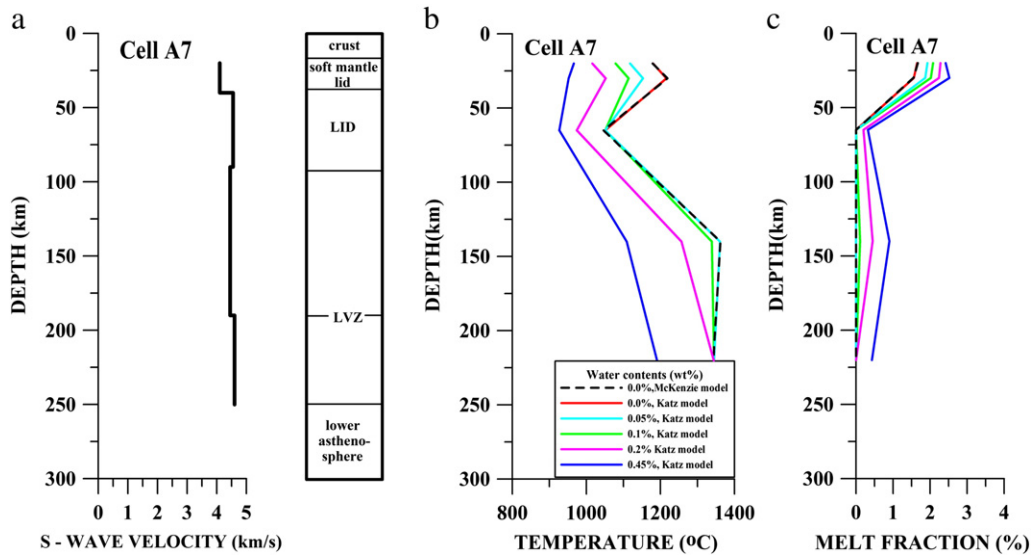


Fig. 3. Vs model of cell A7 (a); sensitivity to the water content (wt.%) of the temperature (b) derived from Vs and the melt percentage (c).

the differences between the temperatures estimated for constant and variable Torre Alfina compositional models to increase with increasing seismic velocity. The same effect is seen if a variable composition containing larger amount of hydrous phases (like Finero composition) is used. The compositional variability produces differences in the inferred temperatures, which reach a maximum value of about 370 °C. In both tests, the melt fraction has the general tendency to decrease by an amount varying between 0.3% and 1%. At 250 km of depth, outside the stability limit for phlogopite, the temperatures estimated for constant and variable compositional models are practically the same. This aspect emphasizes the importance of a realistic choice of the amount and type of hydrous phases composing the upper mantle.

As a conclusion, the capability of inferring plausible temperatures by the developed conversion technique depends on how precisely are evaluated input parameters, like DVC values, weight fraction of water dissolved in the melt and mantle composition variability.

3. Results

For the cross-sections 1–4 (see in Fig. 1b their location), the conversion of the Vs cellular model into temperature profile (geotherm)

for each cell along the sections is performed following the procedure described in Section 2. The full description of all relevant parameters is given for each cell analysed in Appendix D. One temperature value and the corresponding melt fraction at the middle of each layer of the upper mantle (from Moho to about 300 km depth) are obtained by the conversion of average velocity. To stabilize the plotting routine, at 1/4 and 3/4 of the cell width the temperature and corresponding melt fraction are assumed equal to the values estimated at the middle of the cell. The temperatures in the crust, at Conrad and Moho levels, are calculated using a simple 1-D thermal model. The ranges of variation for the thermal parameters (thermal conductivities and heat generation) are compiled from literature (mainly from Artemieva and Mooney, 2001) and given in Appendix C.

In the modelling, in each cell the composition is laterally homogeneous, but the homogeneous composition may differ from cell to cell. For cells located in front of the present-day convergence fronts (see Fig. 1b) temperature and melt fraction values in the upper mantle are obtained using the Finero type reference mantle composition (Table 2), the mean sensitivity to the presence of melt, DVC = 4 and variable depth water content, i.e., a large value of 0.45 wt.% in the depth interval from Moho to the stability limit of phlogopite, taken

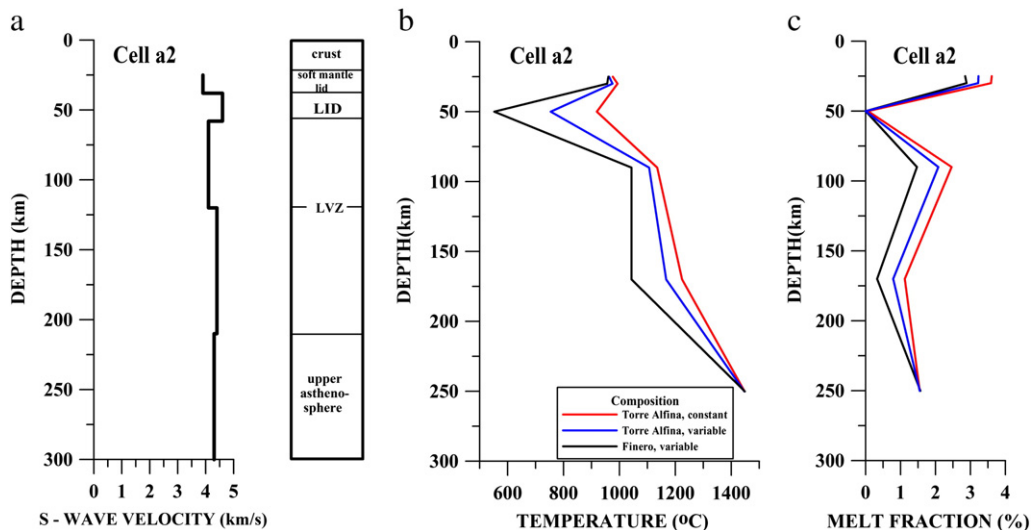


Fig. 4. a2 cellular model (a); sensitivity to variation of mantle composition of the temperature derived from Vs (b) and of the melt percentage (c).

equal to 200 km, and a small value of 0.1 wt.% at depths larger than 200 km. In case of cells located in foreland areas, the mantle composition, defined following Table 3, remains fixed with depth and a smaller value of water content of 0.1 wt.% is assumed (but DVC is kept equal to 4).

The temperature ((colour) scale) and melt fraction (isolines) distributions along the cross-sections from 1 to 4 are plotted in Figs. 5 to 8. In all cross-sections the (colour) scale of temperatures starts at 11 °C, assumed as average surface temperature in Italy.

3.1. Section 1: Southern Sardinia–Eastern Aeolian Arc–Southern Calabria–Ionian Sea (cells B-2 to B4, C5 to C7, D7)

Section 1 is a representative profile for the Central-Southern Tyrrhenian Sea and runs from southern Sardinia to the Aeolian arc and Calabria, following the direction of maximum extension of the Tyrrhenian basin (Sartori, 2003). The main aspects of the thermal structure along this section (Fig. 5) can be summarized as follows:

- (1) a thick, relatively cool zone beneath the eastern Aeolian Arc and Calabria (cells C5, C6), which extends to depths of more than 150 km;
- (2) a deep thermal influence of the cool zone, with downward inflection of isotherms;
- (3) the uppermost mantle to the west of the cool zone is relatively cold, with temperatures below 1000 °C; however, a relatively hot layer is seen beneath the Tyrrhenian basin (cells B1–B4) centred at about 30 km of depth, and a confined hot zone beneath cell B4 at a depth of about 100 km. The geothermal gradient in the back-arc basin is much less steep than that modelled for mantle wedges and back-arc areas behind very steep westward directed subduction zones (Carminati et al., 2005);
- (4) there is a strong rise of the isotherms in the foreland where the highest thermal gradient is seen;
- (5) 1% melt is seen at about 100 km depth, while a hot layer containing up to 4% melt is present at shallower levels. Only about 0.5% melt is present beneath the foreland.

3.2. Section 2: Northern Sardinia–Southern Apulia (cells A-2 to A8)

The section runs along the so-called 41° parallel line, a main tectonic structure that divides Tyrrhenian basin into its northern and southern sectors, each characterized by different degree of extension and intensity and type of volcanic activity (Bruno et al., 2000). The volcanism of the Pontine Islands (from 4.5 Ma to less than 1 Ma ago) and the active Campania Province (Ischia, Campi Flegrei,

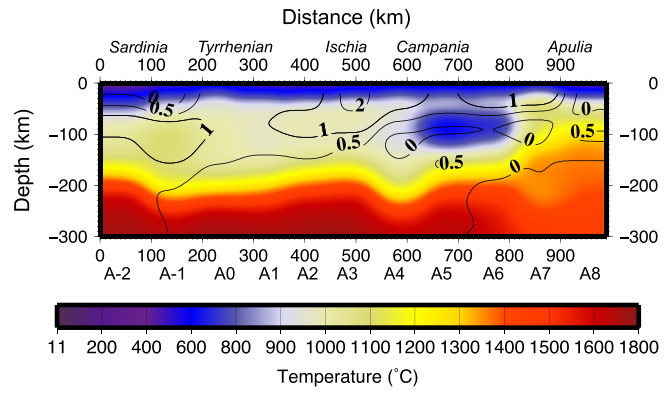


Fig. 6. Temperature and melt fraction (isolines) distribution along cross-section 2.

Vesuvio) are located along this line. Several interesting features are seen in the thermal structure of the section shown in Fig. 6:

- (1) a negative thermal anomaly extends horizontally from the active volcanic area of Vesuvio and Campi Flegrei until the western border of Apulia; such a cold zone is approximately 100 km thick and ends abruptly against the border of the foreland (cell A7);
- (2) a slight perturbation of temperatures beneath the cold zone, with waving of isotherm;
- (3) a zone of relatively less-cold mantle extends west of this negative thermal anomaly (until cell A1) and occupies the entire sub-Tyrrhenian uppermost mantle; a zone of relatively hotter material beneath the cell A-1, is possibly related to local rifting process and volcanism in northern Sardinia (Della Vedova et al., 2001);
- (4) the temperatures in the back-arc area, significantly higher in Section 1 than in Section 2, are in natural agreement with the relatively stronger degree of extension in the southern Tyrrhenian Sea; the highest thermal gradients, in comparison with those of the back-arc area, with temperatures as high as 1000 °C, observed at a depth of only 30–40 km (i.e. Moho depth), are seen in the foreland;
- (5) the melt distribution is only roughly related to temperatures and it is different when compared with that shown in Section 1; about 2% melt is present beneath Ischia (cell A3) whereas the 1% melt isotherm is present at about 100 km of depth and rises at about 50 km going eastward.

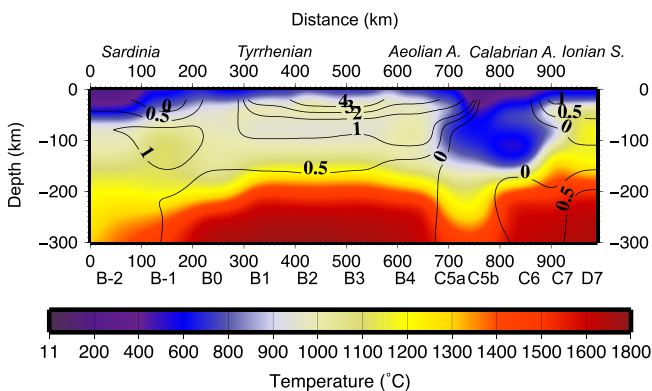


Fig. 5. Temperature and melt fraction (isolines) distribution along cross-section 1.

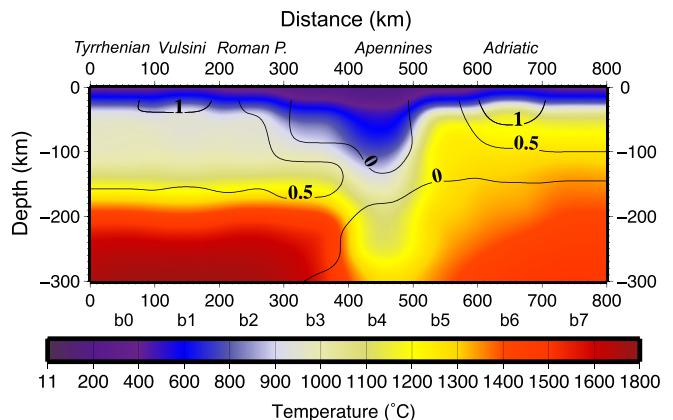


Fig. 7. Temperature and melt fraction (isolines) distribution along cross-section 3.

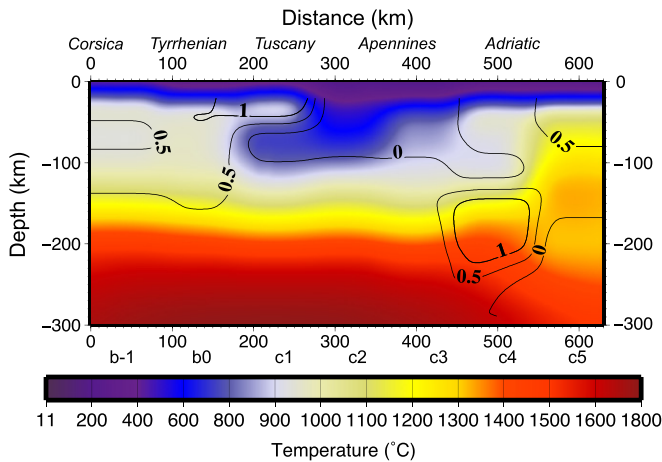


Fig. 8. Temperature and melt fraction (isolines) distribution along cross-section 4.

3.3. Section 3: Central Tyrrhenian Sea – Latium–Umbria–Marche–Adriatic Sea (cells b0 to b7)

This section starts from the back-arc basin, reaches the Roman Province and, then, crosses the Apennines chain (cells b3, b4) to finally reach the Adriatic foreland (cells b5–b7).

The main features seen in this section (Fig. 7) are:

- (1) a relatively thick layer of cold material centred at the boundary (cell b4) between the Apennines chain and the Adriatic foreland;
- (2) deep thermal modifications seem to be absent beneath the back-arc basin and the Roman province (cells b0 to b2), whereas they are very strong beneath the Apennines and the western margin of the Adriatic foreland;
- (3) there is an important rise of the isotherms beneath the foreland, where temperatures of about 1100 °C are reached at a depth of less than 50 km;
- (4) melt distribution is about 1% at depths of 30–40 km in the western part of the section beneath the back-arc basin (cell b0) and the Vulsini volcanic complex (cell b1), whereas the same value is observed at a depth of about 50 km beneath the Adriatic plate (cell b6).

3.4. Section 4: Northern Tyrrhenian Sea – Tuscany–Umbria–Adriatic Sea (cells b-1, b0, c1 to c5)

This section (Fig. 8) crosses the northern end of the Miocene–Quaternary volcanic belt of the Italian peninsula, from Corsica to Tuscany, northern Umbria and the Adriatic Sea. Main features are:

- (1) a cold zone, from just below the Moho to about 100 km depth, extends horizontally from southern Tuscany to the border of the Adriatic Sea (cells c1–c3); a small zone of relatively hotter material separates the crust from the cool body beneath southern Tuscany (cell c1);
- (2) beneath the negative thermal anomaly, isotherms run parallel from cell c3 to the western cells;
- (3) as in Fig. 7, isotherms rise beneath the foreland (cell c5);
- (4) melt is generally present in small quantities (less than 1%); more than 1% melt (1.7–1.8%), at a depth of about 30 km, is seen beneath Tuscany area (cell c1), in accordance with magmatic activity generating local thermal anomalies and systems (Della Vedova et al., 2001) and young volcanism (e.g. Mt. Amiata, 0.3 Ma old) and at a depth of about 150 km beneath the Adria plate.

4. Discussion

Some of the features mentioned in Sections 3.1–3.4 are rather obvious, fit current models of the evolution of the Tyrrhenian Sea area and therefore represent a positive test of the validity of the enhanced procedure. Others are more problematic, and deserve some in-depth discussion.

4.1. Influence of the assumptions made on mantle composition and water content on the temperature's field

To understand which characteristics of the temperature's field are real features or artefacts of our choice for the mantle composition, considering Section 1, a parametric test of the effect of changing the representative composition for the back-arc area has been performed. If in the back-arc region, the Finero type composition is replaced by the (variable) Torre Alfina type composition (Table 2), the main features of the temperature's field (Fig. 9) remain qualitatively similar to the (previous) model reported in Fig. 5.

This result is in accordance with the results of the parametric test, displayed in Fig. 4, on the sensitivity of inferred temperatures to the mantle composition: the larger amount of hydrous phases (like Finero type composition) produces lower temperatures; there is a tendency to increase the differences between the estimated temperatures with increasing seismic velocities in the cold zone. The clear tendency of the temperatures derived from Vs to decrease, when a composition containing a larger amount of hydrous phases (like Finero composition) is considered, partially explains the common feature of all sections, i.e., the temperatures inferred by Vs–T conversion are overall lower in the back-arc area than in the foreland. However, this characteristic is also the effect of the large water content of 0.45 wt.%, assumed in the upper 200 km of the mantle, for the cells located in the back-arc areas, in comparison with the foreland region, where a smaller water content of 0.1 wt.% is assumed. The cooler back-arc seems to be a real feature because the results of the thermal modelling are based on assumptions (concerning the water content distribution in the upper mantle) which are well documented by the composition of the upper mantle in this area. The sensitivity test presented in Fig. 3 indicates that a higher water content in the mantle rocks (of 0.45 wt.%) reduces the calculated temperature values by 12–22% and increases melt fraction values by more than 47%. At depths of 200–300 km, in absence of hydrous phases, the temperatures inferred by Vs–T conversion are similar in the back-arc area and in the foreland (see cross-section 1), despite the difference in the mantle composition of the two regions. The above-mentioned aspects could be interpreted

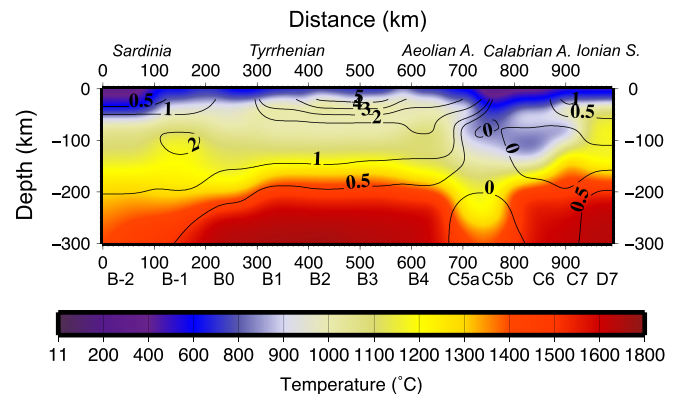


Fig. 9. Variant of the temperature and melt fraction (isolines) distribution for Section 1, obtained using (variable) Torre Alfina type composition for the back-arc area.

as the evidence that the temperatures derived from Vs have a stronger sensibility to the water content than to the mineralogy variability. Obviously, the influence of water content diminishes when small water contents are assumed. Consequently, when in the modelling, at depths larger than 200 km, the water content of 0.1 wt.% has been replaced by 0.01 wt.%, the temperature's field does not change significantly. On the contrary, at depths larger than 200 km, the use of implausible large water content of 0.45 wt.% instead of 0.1 wt.% converts into a general decrease of the temperature evaluations by more than 200 °C.

The overall uprise of the isolines in the foreland in comparison to the back-arc basin is a rather surprising result. It seems that the asthenospheric uprise in the back-arc was insufficient to counterbalance the effect of cooling generated by subduction, at least in the northern and central Tyrrhenian area, because of the low extension rate there. This phenomenon is less strong in Section 1, where the back-arc extension is stronger and the relatively hotter temperatures may indicate inflow of asthenospheric mantle toward the subduction zone. A very speculative explanation for the fact that temperatures are overall lower in the back-arc area than in the foreland, can well be in agreement with the eastward mantle flow (Panza et al., 2007b), that causes the hot material to be somehow trapped under the Ionian/Adria lithosphere, see the relatively high melt fraction at about 150 km of depth in cell c4 in cross-section 4, whose eastern margin is subducting at low angle under Dinarides/Balkans (Brandmayr et al., 2010, 2011). Matter for an alternative interpretation is supplied by Zhu et al. (2011) who point out that low fraction of melts ≤ 1 wt.% cannot rise in compressive regimes and thus may cause high temperatures under Ionian/Adria.

4.2. Temperature models in relation with the heat flow determinations

A consistent justification for the overall uprise of the isotherms in the foreland, which is clearly seen in all the cross-sections, could be obtained by examining, along the cross-sections, the temperature distribution at Moho depth. Temperature values at Moho (reported in Appendix D) seem to be correlated with surface heat flow determinations in the Tyrrhenian Sea area and surroundings, provided by Pasquale et al. (1996) and Della Vedova et al. (2001). Heat flow is considered as the surface expression of major tectonic processes affecting the thermal regime of the lithosphere. In this analysis we take into account that most of the provinces of the study area (like Tuscan–Tyrrhenian area, Apennines and Adriatic trough) have not reached the steady-state thermal regime and, consequently, advective/convective heat transfer by processes like meteoric water infiltration, recent sediment deposition, igneous intrusions, could affect the predicted surface heat flow values (Della Vedova et al., 2001). In the area of maximum extension of the Tyrrhenian basin (Section 1, cells B1–B4, Fig. 5), characterized by the highest heat flow values (at least 150 mWm^{-2}), temperatures reach large values (about 1025 °C for cell B4) at Moho depth, which varies between 11 and 14 km. Low temperatures are observed at the western end of Section 1 (cell B-2) and in the continental convergence zone (cells C5b, C6), where heat flow values are below the continental average values (which range from 55 to 65 mWm^{-2} , according to Jessop et al., 1976; Sclater et al., 1980; Jaupart and Mareschal, 2007). Similar scenarios are obtained for the Sections 2, 3 and 4 (Figs. 6 to 8): temperatures around 950 °C at rather small Moho depths (of 20–30 km) in the back-arc zone, correspond to large heat flow values (about $100\text{--}150 \text{ mWm}^{-2}$) as well as in the foreland (cells A7, A8), where heat flow is between 40 and 50 mWm^{-2} ; low temperatures at large Moho depths (of around 40 km) in a continental convergence region (cells b3, b4) correspond to low heat flow, but the highest temperatures (varying between 1040 and 1075 °C) in the foreland (cells b5–b6), characterized by local high heat flow (about 80 mWm^{-2}), point out an extensional tectonic regime (rifting indicated by Brandmayr et al., 2010). In case of

Section 4, the high temperatures at Moho depth in the foreland area (cell c5) are difficult to be correlated with heat flow determinations, which indicate slightly low values, probably affected by the recent sediment deposits in the Adriatic trough (Della Vedova et al., 2001).

In spite of an overall correspondence between temperatures at Moho and surface heat flow values, a detailed comparison between measured surface heat flow values and those inferred from thermal gradients at Moho depth is not appropriate. Such a comparison is meaningful in stable tectonic continental areas where it is reasonable to assume that the heat propagates by conduction in the vertical direction (1-D steady-state conduction model) through the lithosphere. The 1-D thermal model obviously cannot model the physics of heat conduction in active tectonic areas, where the advective and the convective heat transfer (by movement of solid or fluid material) have to be taken into account and, consequently, the surface heat flow in areas experiencing recent tectonic processes deviates from the values pertinent to a steady-state heat flow.

4.3. Thermal models and their geodynamic significance

Relatively low temperatures (negative thermal anomaly), observed in all sections along the Apennines chain and the Calabrian block, clearly mark the subducting slab. Different geometries and extension of these anomalies reflect distinct evolutionary stages for subduction. The vertical geometry of the slab beneath Calabria and the Aeolian arc (Section 1, cells C5, C6, Fig. 5), as well as in Umbria (Section 3, cells b3, b4, Fig. 7) is in agreement with the high dipping angle of west-directed subduction zones seismically detected in the southern Tyrrhenian Sea and at a global scale (Caputo et al., 1970, 1972; Doglioni et al., 1999; Riguzzi et al., 2010). The horizontal extension of the cool zone beneath the Tuscany area (Section 4, cell c1, Fig. 8) and northern Umbria (cells c2–c3) may be an indicator of the fact that the subduction is not very active in this region (the case of continental collision) and that the slab may be rather floating, instead of sinking into the upper mantle. This is consistent with the existence of a light continental-type subducting crust (lithosphere), as indicated by magmatological evidences (i.e. high quantities of ultrapotassic magmas with crustal-like isotopic signatures; Peccerillo, 2005 and references therein) and by recent gravity modelling of the lithosphere–asthenosphere system of the study area (Brandmayr et al., 2011). The features of the thermal model in this area could suggest a process of continental convergence in successive stages of evolution: an older stage beneath Tuscany and a younger one beneath northern Umbria, as a result of the eastward migration of the compression front. Therefore, the horizontal relatively cool layer beneath Tuscany–Umbria area is interpreted as generated by subduction of continental plate, decrease of tectonic push on the slab and its flattening due to density contrast with the ambient upper mantle. Such a model explains the so-called “crustal doubling”, suggested by various authors (e.g. Scrocca et al., 2003; Pauselli et al., 2006 and references therein) and the uplift of central Apennines, a consequence of the isostatic adjustment related to slab floating. A flattened Adriatic slab, which cannot undergo gravitational subduction, i.e. slab pull (Brandmayr et al., 2011), but rather is dragged to some depth by the eastward mantle flow (Panza et al., 2007b) supplies a quite natural explanation of the phenomenon.

A flat cool zone is observed in Campania (Section 2, cells A5, A6, Fig. 6) too. Here, the cool zone cannot represent the actively subducting Ionian slab, which defines a narrow Benioff zone extending from the eastern Aeolian arc until Campania, where a depth around 500 km is reached. According to several models (e.g. Doglioni et al., 1999; Carminati et al., 2005 and references therein) there was a continuous Adriatic–Ionian plate subducting beneath southern Apennines and Calabria, until recently. According to Peccerillo (2001, 2005) and Panza et al. (2007a), the latest stages of subduction convergence were characterized by tear-off of the Ionian–Adriatic slab caused by the stoppage of the subduction in the Adriatic sector and the continuance of slab

sinking in the Ionian sector. Therefore, the cool horizontal zone beneath the Campania area could represent the remnant of the subducted Adriatic plate, which did not sink into the upper mantle because of its low density (Brandmayr et al., 2011), as in the case of Tuscany. The thermal models simulating the subduction process, followed by a thermal relaxation after subduction cessation, indicate the broadening of isotherms (Toksöz and Bird, 1977). The downward deflection of the 1400 °C isotherm beneath cell A4 could be considered the persisting thermal effect of the Adriatic plate subduction or as an effect of the subducted Ionian plate.

The thermal structure of the shallow upper mantle inferred by Vs–T conversion indicates temperature values getting above 1600 °C at the bottom of the sections (300 km). These results seem to be in accordance with the LLAMA (Laminated Lithologies with Aligned Melt Accumulations – the low-velocity anisotropic layer) model proposed by Anderson (2010), who concludes that temperature can be as high as 1600 °C at the base of the boundary layer (BL) and ~200 °C hotter than the ridge geotherm. Our thermal evaluations are not supportive of the assumptions of McKenzie and Bickle (1988) who presume a subsolidus potential temperature of 1280 °C ± 20 °C for ‘ambient mantle’ beneath the plate. In McKenzie and Bickle (1988) model the ambient mantle temperatures, inferred from MORB temperatures obtained by petrological experiments, are forced to approach the ridge geotherm and the mantle cannot retain the melt. Consequently, the seismic low-velocity layer (LVL) is subsolidus and controlled by high temperature gradients with no partial melting (e.g. Priestley and McKenzie, 2006). If mid-ocean ridges exemplify the ‘ambient mantle’, the mid-plate magmas seem to require temperatures more than 200 °C higher than the assumed ambient temperatures. Moreover, an upper mantle kept isothermal and homogeneous below the plate could be in disagreement with the Vs heterogeneity in the upper 200 km of the upper mantle, which could exceed 7%, implying temperature variations of 700 °C. Recent geophysical data, like observations on the maximum depths of melting and inferred temperatures of the mid-plate magmas, the models for bathymetry data, the mantle potential temperatures derived from petrology for dry back-arc basin basalts by Kelley et al. (2006) indicate a mean mantle temperature that is higher than that assumed by the McKenzie and Bickle (1988) model and confirm that MORB-source mantle and mid-plate mantle temperatures differ by ~200 °C. Anderson (2010) reconsidered the nature and origin of the LVL and proposed the boundary layer model (LLAMA) for mid-plate magmatism, in which the decrease of seismic velocity with depth is controlled by the high

thermal gradient and the variation of the number and thickness of the small grain areas (shear zones), which concentrate the melt.

4.4. Melt distribution and relation with magmatism

In the back-arc area of the investigated region the modelled melt distribution is approximately correlated with the age of the magmatism (Fig. 10). In Tuscany there is a relatively small amount of melt (around 1.7% at depth of 30 km), and the magmatism is extinct from about 1 Ma, except for Mt. Amiata, which is 0.3 Ma old. Melt fraction is about 1% at shallow depth beneath Vulsini volcano, which has been active until 0.15 Ma bp.

In the volcanic active Campania region, melt amount increases, and wide zones containing 1–2% melt are observed at rather shallow depth. Finally, melt amounts in the southern Tyrrhenian Sea are the highest, in accordance with the occurrence of abundant active volcanism. Large amounts of magmas at shallow depths in back-arc position (cells B1–B3) may result from the accumulation from below and/or mantle inflow and decompression melting. The 1–2% melt fraction at depth under Italy is essentially what Anderson (2010) gets for LLAMA in the oceanic LVZ and it is plenty to make the largest igneous province, but melt eruption occurs when laminar flow in the boundary layer is dislocated.

Melt amounts in the foreland are not significant and only in a few cases values around 1%, comparable to those of back-arc areas, are obtained. Yet, there is no evidence of recent magmatism in the foreland, except for Mount Vulture (0.8 to 0.1 Ma), which is located at the boundary between Apulia foreland and the southern Apennines, just north of Section 2. The occurrence of volcanism is the effect of two causes: sufficient amount of melt available in the source plus extensional tectonic regime (Zhu et al., 2011). Thus, in the offshore Adriatic (Dalmatian islands, cross-section 3, cell b6), the amount of melt around 1% at 50 km of depth, whose possible presence has been mentioned by Brandmayr et al. (2010), seems to be insufficient to produce volcanism, similarly for cross-section 4 in cell c4. A compressional tectonic regime characterizes the contact between the western border of the foreland and the external corrugated chain, and the maximum melt values of 1.6% are observed in Apulia (cell A6), where the Vulture volcano is located.

The synthesis of the characteristics of mantle temperature and melt distributions beneath Italy and surroundings seem to be in accordance with Anderson (2010) who suggests that the upper mantle may be, more often than generally believed, above its solidus and the surface manifestations (like heat flow, volcanism, degassing) of the mantle features are the effect of lithospheric structures and stress regimes rather than the mantle peculiarities.

5. Conclusions

We present thermal models of the upper mantle in Italy and surroundings, along four geotraverses, based on the assumption that the upper mantle seismic structure is controlled both by temperature and composition. The obtained results confirm the possibility to interpret the upper-mantle seismic models in terms of temperature and composition, and offer an enhanced insight into the geodynamic evolution, still in debate, of one of the most studied and geodynamically complex regions of Europe.

Based on the thermal structure and melt distribution obtained, the following conclusions may be drawn: the ongoing subduction process of the Ionian/Adriatic plate (beneath Umbria, Calabria and the Aeolian arc), the latest episode of continental convergence (beneath Tuscany) and the thermal effect of the remnant of the Adriatic plate (Campania) leave distinctive signatures in the temperature’s field of the shallow upper mantle. Despite the epistemic uncertainties in the temperature–seismic velocity conversion technique, which affect the thermal estimations, the temperature field characteristics seems to be in agreement

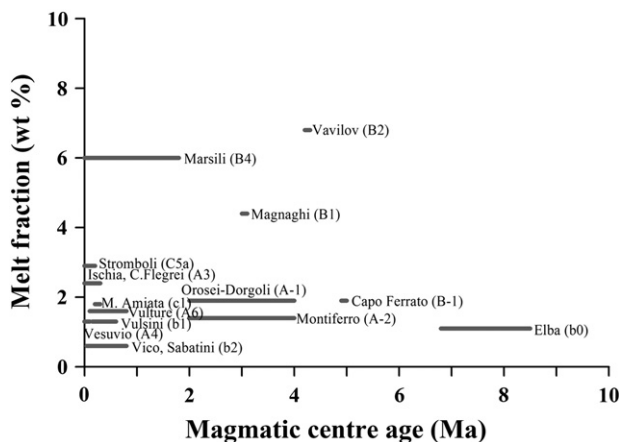


Fig. 10. Correlation between the melt fraction (evaluated for the main volcanic areas) with the age of the magmatism. Cell numbers of different centres (Fig. 1b) are given in parentheses.

with independent studies about the change of the slab structure along the Apennines chain, from north to south, due to fragmentation of Apennines' lithosphere with the gradual termination of active subduction: in the Northern Apennines the slab is almost horizontal, and underlies the chain and the uplift of Apennines is the result of the isostatic adjustment. In the Central Apennines the slab is almost vertically dipping and reaches depths of around 130 km, whereas beneath the Southern Apennines the slab reaches larger depths, its dynamics being controlled by roll-back and tearing processes (Panza et al., 2007a).

Temperature values at Moho are, in general, correlated with surface heat flow values in the Tyrrhenian Sea area and surroundings, even if most of the provinces of the study area (like Tuscan-Tyrrhenian area, Apennines and Adriatic trough) have not yet reached the steady-state thermal regime. The thermal gradients evaluated in Adria foreland are higher in comparison with those of the back-arc area (Tyrrhenian Sea) and they could be an effect of the eastward mantle flow (Panza et al., 2007b) beneath Adria lithosphere or a consequence of the presence of a low fraction of melts ≤ 1 wt.%, which cannot rise in the compressive regimes, or both.

Melt fraction distribution in the back-arc area, corresponding to temperatures inferred by conversion technique, is approximately correlated with the age of the magmatism, the highest abundance occurring in the most active volcanism area in the southern Tyrrhenian Sea.

Acknowledgments

The authors are grateful to Prof. R.F. Katz for kindly sharing the code for the parameterization of melt fraction, used in our study to improve the seismic–temperature conversion procedure. We thank Prof. Don L. Anderson for encouraging remarks on an early version of the paper. We acknowledge partial support from PRIN/2008BYTF98. This research has benefited of the grant “Studio della struttura della crosta e del mantello superiore dell'area mediterranea mediante metodologie sismologiche di inversione non lineare” from Dipartimento di Geoscienze dell'Università degli Studi di Trieste, funded by the Italian Ministero dell'Istruzione, dell'Università e della Ricerca PRIN/2008BYTF98 and Italian PNRA (2004/2.7–2.8) “Sismologia a larga banda, struttura della litosfera e geodinamica nella regione del Mare di Scotia”. This research has been partly developed in the framework of the ASI-Pilot Project “SISMA: SISMA-Information System for Monitoring and Alert”. Part of the figures have been plotted using GMT (Generic Mapping Tools; Wessel and Smith, 1995).

Appendix A

Table A.1

Elastic parameters of the mantle minerals, used in the modelling.

Mineral	Units	Olivine	Orthopyroxene	Clinopyroxene	Garnet	Spinel	Phlogopite	Amphibole
ρ	kg/m ³	3222	3215	3277	3565	3578	2820	3200
K	GPa	129	109	105	171	198	50	55
μ	GPa	81.00	75.00	67.00	92.00	108.00	25.20	34.73
$\delta\rho/\delta X$	10 ³ kg/m ³	1.182	0.799	0.380	0.760	0.702	1.300	1.300
$\delta K/\delta X$	GPa	0	20	12	15	12	0	0
$\delta\mu/\delta X$	GPa	−31	10	−6	7	−24	−28	−28
$\delta K/\delta T$	10 ^{−3} GPa/K	−17	−27	−13	−19	−28	−20	−20
$\delta\mu/\delta T$	10 ^{−3} GPa/K	−14	−12	−10	−10	−12	−11	−11
$\delta K/\delta P$		4.20	7.00	6.20	4.40	5.70	8.59	8.59
$\delta\mu/\delta P$		1.40	1.60	1.70	1.40	0.80	0.77	0.77
α_0	10 ^{−4} K ^{−1}	0.2010	0.3871	0.3206	0.0991	0.6969	0.5800	0.5800
α_1	10 ^{−7} K ^{−2}	0.13900	0.04460	0.08110	0.11650	−0.01080	−0.01742	−0.01742
α_2	10 ^{−2}	0.1627	0.0343	0.1347	1.0624	−3.0799	−1.3000	−1.3000
α_3	K	−0.3380	−1.7278	−1.8167	−2.5000	5.0395	0.9620	0.9620

The values for the elastic parameters of the mantle minerals are compiled from: Goes et al. (2000); Cammarano et al. (2003) (for olivine, orthopyroxene, clinopyroxene, garnet and spinel) and from: Anderson (1988); Anderson and Isaak (1995); Cammarano et al. (2003); Hacker et al. (2003); Pavese et al. (2003); Kopylova et al. (2004); Anderson (2007); Phan (2008); Ji et al. (2009) (for phlogopite and amphiboles).

Appendix B

The Voigt–Reuss–Hill (VRH) averaging scheme is a simple procedure to estimate the elastic constants of a rock in terms of the elastic constants of the constituting minerals, by taking the average of the mean elastic parameters for a constant stress (Reuss) and a constant strain (Voigt) throughout the rock:

$$\langle M \rangle = \frac{1}{2} (M^{\text{Reuss}} + M^{\text{Voigt}}) \quad (\text{B.1})$$

$$M^{\text{Reuss}} = \left(\sum \frac{\lambda_i}{M_i} \right)^{-1}; M^{\text{Voigt}} = \sum \lambda_i M_i \quad (\text{B.2})$$

where $\langle M \rangle = \mu$ (for S-wave velocities) or $K + (4/3)\mu$ (for P-wave velocities), $M_i = \mu$ or K and λ_i is the volumetric proportion of mineral i .

The density of a rock consisting of i minerals can be expressed as follows:

$$\langle \rho \rangle = \sum \lambda_i \rho_i \quad (\text{B.3})$$

To calculate the partial derivative of the seismic velocity V (anharmonic part) the equations for the VRH averaging scheme are differentiated and give the following expressions:

$$\left(\frac{\partial V}{\partial T} \right) = \left[\frac{\partial \langle M \rangle}{\partial T} - v^2 \frac{\partial \langle \rho \rangle}{\partial T} \right] / [2 \langle \rho \rangle V] \quad (\text{B.4})$$

where:

$$\begin{aligned} \frac{\partial \langle \rho \rangle}{\partial T} &= \sum \lambda_i \frac{\partial \rho_i}{\partial T} \text{ and } \frac{\partial \langle M \rangle}{\partial T} \\ &= \frac{1}{2} \left(\sum \lambda_i \frac{\partial M_i}{\partial T} + (M^{\text{Reuss}})^{-2} \sum \frac{\lambda_i}{M_i^2} \frac{\partial M_i}{\partial T} \right) \end{aligned} \quad (\text{B.5})$$

Appendix C

In stable tectonic regions, like old continental platforms and shields, the heat propagates through the lithosphere by conduction, in a

steady-state regime and in the vertical direction; therefore the temperature can be evaluated by the steady state solution of the heat equation:

$$\frac{\partial}{\partial z} \left(k(z,T) \frac{\partial T}{\partial z} \right) = -H(z) \quad (C.1)$$

with boundary conditions at the surface:

$$T(z = 0) = T_0 \quad (C.2)$$

$$q_0 = -k \frac{\partial T}{\partial z} \Big|_{z=0} \quad (C.3)$$

where $k(z, T)$ is the thermal conductivity as a function of composition and temperature, $H(z)$ is the heat production as a function of depth, q_0 is the average value of the near-surface heat flow for the study area and T_0 is the mean annual temperature in the region. For a multilayered lithosphere (Fig. C.1) the solution of this boundary value problem is a simple analytical relationship (1-D thermal model) which allows us the evaluation of temperatures within the crust and lithospheric mantle from surface heat flow q_0 (by the downward continuation technique), if a priori information on the distribution of thermal parameters (thermal conductivity and heat production) together with data on the crustal structure are known. In Fig. C.1 we present a schematic 1-D thermal model (thermal parameters and corresponding steady-state solution) for each layer of the stratified lithosphere.

In our study, following Čermák et al. (1991), the thermal conductivity in the upper crust is considered temperature-dependent according to:

$$k(T) = k_0 / (1 + CT) \quad (C.4)$$

where k_0 is the thermal conductivity at room temperature and C is a temperature correction for thermal conductivity. The exponential depth-dependence of the heat production in the enriched upper crust, $H(z) = H_0 \exp(-z/D)$, proposed by Lachenbruch (1970), has been also taken into account. The characteristic depth D , interpreted as the thickness of a layer with a uniform radioactivity (approximately limited to the upper crust) could be obtained from a linear relationship between surface heat flow q_0 and near-surface radioactivity H_0 . Table C.1 contains the values of the thermal parameters used in the thermal modelling.

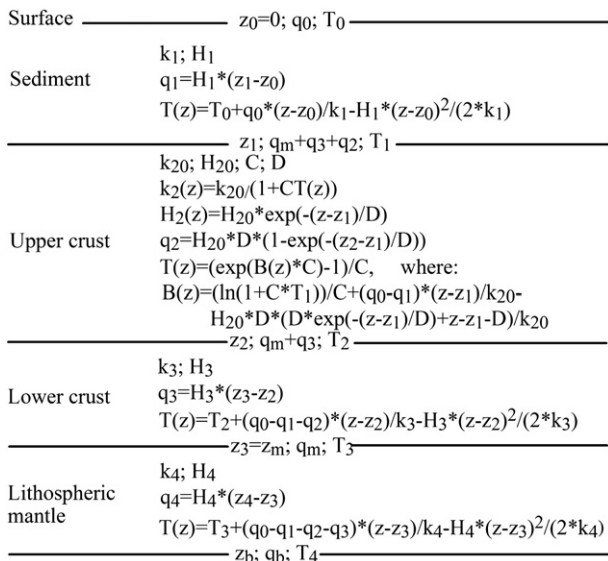


Fig. C.1. Schematic 1-D thermal model: the thermal parameters (k and H) and the corresponding steady-state solutions $T(z)$ for each layer.

Table C.1 Thermal parameters.

Parameter	Units	Sediment	Upper crust	Lower crust	Upper mantle
Thermal conductivity	$Wm^{-1} K^{-1}$	2.5	2.7	2.0	4.0
Heat production	$10^{-6} Wm^{-3}$	0.80	0.90	0.20	0.01
Temperature correction C	K^{-1}	0	0.001	0	0
Characteristic depth D	$10^3 m$	–	16	–	–

For a steady state conduction model, q_0 is the sum of two terms: heat flowing into lithosphere from its base, q_b , and the heat generated by radioactive decay within lithosphere. The heat generated in the lithospheric mantle is insignificant (H_4 is negligible) in comparison with the heat generated in the crust q_c (where $q_c = q_1 + q_2 + q_3$). Consequently, q_b is considered equal to q_m (heat at Moho depth) and $q_0 \approx q_m + q_c$.

Appendix D

Section 1 (Finero) (Fig. 5)

B-2				B-1			
Depth (km)	V_{Sref} (km/s)	T (°C)	Melt (%)	Depth (km)	V_{Sref} (km/s)	T (°C)	Melt (%)
–2		33					
–5		65		–2		81	
–15		190		–10		398	
–16	4.70	210	0.0	–19		767	
–25	4.70	232	0.0	–20	4.40	814	0.0
–61	4.20	943	1.4	–44	4.40	866	0.0
–115	4.30	991	0.7	–95	4.00	1103	1.9
–192	4.30	1185	0.6	–195	4.35	1151	0.5
–242	4.30		0.6	–269	4.35		0.5
B0				B1			
Depth (km)	V_{Sref} (km/s)	T (°C)	Melt (%)	Depth (km)	V_{Sref} (km/s)	T (°C)	Melt (%)
–3		134		–4		263	
–8		370		–5		340	
–19		906		–13		960	
–20	4.30	947	0.6	–14	3.60	995	4.4
–50	4.30	929	0.8	–20	3.60	993	4.4
–110	4.25	1012	0.9	–57	4.20	936	1.4
–180	4.40	1069	0.3	–130	4.30	1031	0.7
–255	4.40	1619	0.3	–210	4.40	1530	0.2
–290	4.40		0.4	–252	4.40		0.3
B2				B3			
Depth (km)	V_{Sref} (km/s)	T (°C)	Melt (%)	Depth (km)	V_{Sref} (km/s)	T (°C)	Melt (%)
–4		327		–4		280	
–5		430		–5		360	
–10		930		–12		940	
–11	4.05	985	1.9	–13	3.80	990	3.3
–14	4.05	974	1.9	–15	3.80	983	3.3
–20	3.15	1083	6.8	–21	3.10	1095	7.0
–55	4.20	936	1.4	–54	4.20	935	1.3
–130	4.30	1032	0.7	–121	4.30	1007	0.7
–220	4.40	1552	0.3	–215	4.40	1542	0.3
–272	4.40		0.3	–269	4.40		0.3
B4				C5a			
Depth (km)	V_{Sref} (km/s)	T (°C)	Melt (%)	Depth (km)	V_{Sref} (km/s)	T (°C)	Melt (%)
–3		240		–3		160	
–5		420		–7		390	
–11		980		–16		920	
–12	3.30	1024	6.0	–17	3.90	975	2.8
–18	3.30	1047	6.0	–31	3.90	961	2.9
–43	4.20	935	1.3	–71	4.60	607	0.0
–81	4.05	1044	1.7	–147	4.50	900	0.0
–140	4.40	975	0.3				

(continued on next page)

Appendix D (continued)

Section 1 (Finero) (Fig. 7)							
B4				C5a			
Depth (km)	V _{Sref} (km/s)	T (°C)	Melt (%)	Depth (km)	V _{Sref} (km/s)	T (°C)	Melt (%)
-230	4.40	1572	0.3	-237	4.70	1220	0.0
-280	4.40		0.4	-277	4.70		0.0
C5b				C6			
Depth (km)	V _{Sref} (km/s)	T (°C)	Melt (%)	Depth (km)	V _{Sref} (km/s)	T (°C)	Melt (%)
-3		45		-5		116	
-17		90		-19		440	
-43		470		-33		730	
-44	4.60	533	0.0	-34	4.50	765	0.0
-71	4.60	598	0.0	-53	4.50	809	0.0
-147	4.50	892	0.0	-122	4.65	469	0.0
-237	4.70	1210	0.0	-212	4.40	1529	0.2
-277	4.70		0.0	-252	4.40		0.3
C7 (foreland)				D7 (foreland)			
Depth (km)	V _{Sref} (km/s)	T (°C)	Melt (%)	Depth (km)	V _{Sref} (km/s)	T (°C)	Melt (%)
-2		84		-3		120	
-6		240		-6		240	
-25		1060		-24		1015	
-26	4.25	1074	1.4	-25	4.40	1026	0.7
-40	4.25	1122	1.3	-47	4.40	1100	0.6
-74	4.80	748	0.0	-82	4.45	1187	0.3
-137	4.50	1311	0.0	-137	4.60	1159	0.0
-220	4.45	1530	0.1	-220	4.25	1602	0.8
-260	4.45		0.2	-260	4.25		0.9
Section 2 (Finero) (Fig. 6)							
A-2				A-1			
Depth (km)	V _{Sref} (km/s)	T (°C)	Melt (%)	Depth (km)	V _{Sref} (km/s)	T (°C)	Melt (%)
-2		73		-2		73	
-5		170		-10		347	
-16		580		-20		740	
-17	4.55	607	0.0	-21	4.45	850	0.0
-29	4.55	634	0.0	-45	4.45	907	0.0
-65	4.20	954	1.4	-95	4.00	1103	1.9
-141	4.30	1059	0.7	-194	4.35	1147	0.5
-218	4.30	1583	0.6	-261	4.35		0.5
-268	4.30		0.7				
A0				A1			
Depth (km)	V _{Sref} (km/s)	T (°C)	Melt (%)	Depth (km)	V _{Sref} (km/s)	T (°C)	Melt (%)
-3		140		-3		104	
-7		330		-6		203	
-18		900		-25		899	
-19	4.30	949	0.6	-26	4.30	939	0.7
-42	4.30	929	0.8	-42	4.30	930	0.8
-100	4.20	1018	1.1	-84	4.20	970	1.1
-175	4.40	1057	0.3	-155	4.40	1005	0.3
-250	4.40	1610	0.3	-250	4.45	1588	0.1
-293	4.40		0.4	-300	4.45		0.2
A2				A3			
Depth (km)	V _{Sref} (km/s)	T (°C)	Melt (%)	Depth (km)	V _{Sref} (km/s)	T (°C)	Melt (%)
-3		100		-4		145	
-6		190		-12		450	
-25		840		-23		863	
-26	4.40	930	1.0	-24	4.00	958	2.3
-34	4.40	924	0.2	-45	4.00	973	2.4
-68	4.15	987	1.6	-116	4.35	959	0.5
-139	4.35	1010	0.5	-216	4.40	1540	0.2
-226	4.40	1562	0.3	-266	4.40		0.3
-272	4.40		0.3				
A4				A5			
Depth (km)	V _{Sref} (km/s)	T (°C)	Melt (%)	Depth (km)	V _{Sref} (km/s)	T (°C)	Melt (%)
-1		50		-4		170	
-9		400		-9		390	
				-20		900	

Appendix D (continued)

Section 2 (Finero) (Fig. 6)							
A4				A5			
Depth (km)	V _{Sref} (km/s)	T (°C)	Melt (%)	Depth (km)	V _{Sref} (km/s)	T (°C)	Melt (%)
-19		910		-21	4.25	949	0.9
-20	4.20	953	1.1	-44	4.25	932	1.1
-42	4.20	935	1.3	-84	4.60	502	0.0
-105	4.45	902	0.0	-148	4.30	1075	0.7
-199	4.40	1114	0.3	-232	4.45	1552	0.1
-253	4.40		0.3	-272	4.45		0.2
A6				A7 (foreland)			
Depth (km)	V _{Sref} (km/s)	T (°C)	Melt (%)	Depth (km)	V _{Sref} (km/s)	T (°C)	Melt (%)
-3		135		-5		246	
-9		420		-8		416	
-19		900		-19		1035	
-20	4.15	956	1.4	-20	4.10	1079	2.1
-40	4.15	938	1.6	-30	4.10	1114	2.0
-79	4.65	625	0.0	-65	4.55	1051	0.0
-134	4.35	998	0.5	-140	4.45	1339	0.1
-224	4.50	1500	0.0	-220	4.60	1345	0.0
-272	4.50		0.0	-250	4.60		0.0
Section 3 (Finero) (Fig. 7)							
b0				b1			
Depth (km)	V _{Sref} (km/s)	T (°C)	Melt (%)	Depth (km)	V _{Sref} (km/s)	T (°C)	Melt (%)
-7		226		-1		45	
-18		652		-7		271	
-26		917		-22		895	
-27	4.25	942	0.9	-23	4.20	948	1.2
-44	4.25	932	1.1	-32	4.20	939	1.3
-115	4.30	985	0.7	-60	4.35	929	0.6
-218	4.40	1542	0.2	-128	4.30	1024	0.7
-270	4.40		0.3	-221	4.45	1530	0.1
				-265	4.45		0.2
b2				b3			
Depth (km)	V _{Sref} (km/s)	T (°C)	Melt (%)	Depth (km)	V _{Sref} (km/s)	T (°C)	Melt (%)
-2		65		-5		102	
-12		364		-15		290	
-30		900		-42		757	
-31	4.35	931	0.4	-43	4.50	784	0.0
-55	4.35	927	0.6	-70	4.50	848	0.0
-120	4.30	1000	0.7	-133	4.25	1068	0.8
-210	4.40	1527	0.3	-218	4.45	1518	0.1
-268	4.40		0.3	-267	4.45		0.1
b4				b5 (foreland)			
Depth (km)	V _{Sref} (km/s)	T (°C)	Melt (%)	Depth (km)	V _{Sref} (km/s)	T (°C)	Melt (%)
-7		108		-6		167	
-17		224		-16		468	
-40		513		-36		1013	
-41	4.60	526	0.0	-37	4.45	1041	0.5
-71	4.60	599	0.0	-102	4.45	1238	0.2
-156	4.45	981	0.1	-202	4.60	1305	0.0
-246	4.75	1119	0.0	-237	4.60		0.0
-281	4.75		0.0				
b6 (foreland)				b7 (foreland)			
Depth (km)	V _{Sref} (km/s)	T (°C)	Melt (%)	Depth (km)	V _{Sref} (km/s)	T (°C)	Melt (%)

Appendix D (continued)

Section 3 (Finero) (Fig. 7)

b6 (foreland)				b7 (foreland)			
Depth (km)	V _{Sref} (km/s)	T (°C)	Melt (%)	Depth (km)	V _{Sref} (km/s)	T (°C)	Melt (%)
-8		310		-4		127	
-16		708		-21		755	
-24		1044		-30		1032	
-25	4.20	1077	1.6	-31	4.40	1042	0.7
-32	4.20	1101	1.6	-46	4.40	1092	0.6
-69	4.35	1183	0.7	-86	4.35	1233	0.7
-179	4.55	1329	0.0	-171	4.50	1375	0.0
-229	4.55		0.0	-231	4.50		0.0

Section 4 (Finero) (Fig. 8)

b-1				b0			
Depth (km)	V _{Sref} (km/s)	T (°C)	Melt (%)	Depth (km)	V _{Sref} (km/s)	T (°C)	Melt (%)
-4		197		-7		226	
-17		940		-18		652	
-18	4.30	950	0.6	-26		917	
-32	4.30	933	0.7	-27	4.25	942	0.9
-61	4.40	926	0.3	-44	4.25	932	1.1
-108	4.30	971	0.7	-115	4.30	985	0.7
-203	4.45	1492	0.1	-218	4.40	1542	0.2
-263	4.45		0.1	-270	4.40		0.3

c1				c2			
Depth (km)	V _{Sref} (km/s)	T (°C)	Melt (%)	Depth (km)	V _{Sref} (km/s)	T (°C)	Melt (%)
-4		160		-2		40	
-7		285		-10		310	
-21		900		-33		505	
-22	4.10	956	1.7	-34	4.60	513	0.0
-32	4.10	944	1.8	-55	4.60	563	0.0
-63	4.55	715	0.0	-121	4.40	959	0.2
-133	4.40	969	0.3	-221	4.40	1550	0.3
-224	4.40	1558	0.3	-262	4.40		0.3
-268	4.40		0.3				

c3				c4			
Depth (km)	V _{Sref} (km/s)	T (°C)	Melt (%)	Depth (km)	V _{Sref} (km/s)	T (°C)	Melt (%)
-4		87		-6		172	
-17		352		-16		484	
-36		705		-29		860	
-37	4.50	771	0.0	-30	4.40	928	0.1
-64	4.50	835	0.0	-60	4.40	925	0.3
-140	4.35	1009	0.5	-115	4.45	924	0.0
-230	4.45	1544	0.1	-165	4.20	1301	1.9
-270	4.45		0.2	-190	4.20		1.9

c5 (foreland)			
Depth (km)	V _{Sref} (km/s)	T (°C)	Melt (%)
-6		170	
-20		630	
-34		1020	
-35	4.40	1054	0.7
-55	4.40	1119	0.6
-125	4.40	1322	0.3
-205	4.60	1312	0.0
-235	4.60		0.0

Section 1 modified (Torre Alfina) (Fig. 9)

B-2				B-1			
Depth (km)	V _{Sref} (km/s)	T (°C)	Melt (%)	Depth (km)	V _{Sref} (km/s)	T (°C)	Melt (%)
-2		57					
-5		127		-2		93	
-15		402		-10		478	
-16	4.70	418	0.0	-19		914	
-25	4.70	439	0.0	-20	4.40	945	0.5
-61	4.20	979	1.7	-44	4.40	928	0.7
-115	4.30	1088	1.2	-95	4.00	1155	2.5
-192	4.30	1283	1.2	-195	4.35	1260	1.0

Appendix D (continued)

Section 1 modified (Torre Alfina) (Fig. 9)

B4				C5a			
Depth (km)	V _{Sref} (km/s)	T (°C)	Melt (%)	Depth (km)	V _{Sref} (km/s)	T (°C)	Melt (%)
-242	4.30		0.6	-269	4.35		0.5
B0				B1			
Depth (km)	V _{Sref} (km/s)	T (°C)	Melt (%)	Depth (km)	V _{Sref} (km/s)	T (°C)	Melt (%)
-3		134		-4		263	
-8		370		-5		340	
-19		906		-13		960	
-20	4.30	952	1.0	-14	3.60	997	4.8
-50	4.30	933	1.2	-20	3.60	1004	4.8
-110	4.25	1099	1.4	-57	4.20	966	1.7
-180	4.40	1192	0.8	-130	4.30	1130	1.2
-255	4.40	1617	0.3	-210	4.40	1529	0.2
-290	4.40		0.4	-252	4.40		0.3

B2				B3			
Depth (km)	V _{Sref} (km/s)	T (°C)	Melt (%)	Depth (km)	V _{Sref} (km/s)	T (°C)	Melt (%)
-4		327		-4		280	
-5		430		-5		360	
-10		930		-12		940	
-11	4.05	988	2.2	-13	3.80	992	3.6
-14	4.05	978	2.3	-15	3.80	986	3.7
-20	3.15	1065	7.1	-21	3.10	1074	7.4
-55	4.20	960	1.8	-54	4.20	957	1.8
-130	4.30	1130	1.2	-121	4.30	1105	1.2
-220	4.40	1550	0.2	-215	4.40	1539	0.2
-272	4.40		0.3	-269	4.40		0.3

B4				C5a			
Depth (km)	V _{Sref} (km/s)	T (°C)	Melt (%)	Depth (km)	V _{Sref} (km/s)	T (°C)	Melt (%)
-3		240		-3		160	
-5		420		-7		390	
-11		980		-16		920	
-12	3.30	1020	6.4	-17	3.90	977	3.1
-18	3.30	1041	6.4	-31	3.90	980	3.2
-43	4.20	938	1.7	-71	4.60	808	0.0
-81	4.05	1099	2.3	-147	4.50	1029	0.5
-140	4.40	1093	0.8	-237	4.70	1208	0.0
-230	4.40	1571	0.2	-277	4.70		0.0
-280	4.40		0.3				

C5b				C6			
Depth (km)	V _{Sref} (km/s)	T (°C)	Melt (%)	Depth (km)	V _{Sref} (km/s)	T (°C)	Melt (%)
-3		63		-5		136	
-17		314		-19		547	
-43		725		-33		905	
-44	4.60	733	0.0	-34	4.50	923	0.0
-71	4.60	800	0.0	-53	4.50	921	0.2
-147	4.50	1020	0.5	-122	4.65	800	0.0
-237	4.70	1197	0.0	-212	4.40	1527	0.2
-277	4.70		0.0	-252	4.40		0.3

C7 (foreland)				D7 (foreland)			
Depth (km)	V _{Sref} (km/s)	T (°C)	Melt (%)	Depth (km)	V _{Sref} (km/s)	T (°C)	Melt (%)
-2		84		-3		120	
-6		240		-6		240	
-25		1060		-24		1015	
-26	4.25	1074	1.4	-25	4.40	1026	0.7
-40	4.25	1122	1.3	-47	4.40	1100	0.6
-74	4.80	748	0.0	-82	4.45	1187	0.3
-137	4.50	1311	0.0	-137	4.60	1159	0.0
-220	4.45	1530	0.1	-220	4.25	1602	0.8
-260	4.45		0.2	-260	4.25		0.9

References

- Anderson, D.L., 1988. Temperature and pressure derivatives of the elastic constants with application to the mantle. *Journal of Geophysical Research* 93 (B5), 4688–4700.
- Anderson, D.L., 2007. *New Theory of the Earth*, 2nd edn. Cambridge University Press, Cambridge, pp. 94–95.
- Anderson, D.L., 2010. Hawaii, boundary layers and ambient mantle – geophysical constraints. First published online: December 2, *Journal of Petrology*, <http://dx.doi.org/10.1093/ptrology/egq068>.
- Anderson, O.L., Isaak, D.G., 1995. Elastic constants of mantle minerals at high temperature. In: Ahrens, T.J. (Ed.), *Mineral Physics and Crystallography: A Handbook of Physical Constants*. AGU Ref. Shelf, vol. 2. AGU, Washington, D. C., pp. 64–97.
- Artemieva, I.M., 2006. Global $1^\circ \times 1^\circ$ thermal model TC1 for the continental lithosphere: implications for lithosphere secular evolution. *Tectonophysics* 416, 245–277.
- Artemieva, I.M., Mooney, W.D., 2001. Thermal structure and evolution of Precambrian lithosphere: a global study. *Journal of Geophysical Research* 106, 16387–16414.
- Artemieva, I.M., Billien, M., L  v  que, J.-J., Mooney, W.D., 2004. Shear wave velocity, seismic attenuation, and thermal structure of the continental upper mantle. *Geophysical Journal International* 157, 607–628.
- Asimow, P.D., Langmuir, C.H., 2003. The importance of water to oceanic mantle melting regimes. *Nature* 421, 815–820.
- Aubaud, C., Hauri, E.H., Hirschmann, M.M., 2004. Hydrogen partition coefficients between nominally anhydrous minerals and basaltic melts. *Geophysical Research Letters* 31, L20611, <http://dx.doi.org/10.1029/2004GL021341>.
- Beccaluva, L., Bianchini, G., Coltorti, M., Perkins, W.T., Siena, F., Vaccaro, C., Wilson, M., 2001a. Multistage evolution of the European lithospheric mantle: new evidence from Sardinian peridotite xenoliths. *Contributions to Mineralogy and Petrology* 142, 284–297.
- Beccaluva, L., Bonadiman, C., Coltorti, M., Salvini, L., Siena, F., 2001b. Depletion events, nature of metasomatizing agent and timing of enrichment processes in lithospheric mantle xenoliths from the Veneto Volcanic Province. *Journal of Petrology* 142, 173–187.
- Birch, F., 1943. Elasticity of igneous rocks at temperature and pressures. *Geological Society of America Bulletin* 54, 263–286.
- Bolfan-Casanova, N., 2005. Water in the Earth's mantle. *Mineralogical Magazine* 69, 229–257.
- Boyadzhiev, G., Brandmayr, E., Pinat, T., Panza, G.F., 2008. Optimization for non-linear inverse problem. *Rendiconti Lincei* 19, 17–43.
- Brandmayr, E., Raykova, R.B., Zuri, M., Romanelli, F., Doglioni, C., Panza, G.F., 2010. The lithosphere in Italy: structure and seismicity. In: Beltrando, M., Peccerillo, A., Mattei, M., Conticelli, S., Doglioni, C. (Eds.), *The Geology of Italy: Tectonics and Life along Plate Margins*, Electronic edition. *Journal of the Virtual Explorer*, vol. 36, <http://dx.doi.org/10.3809/jvirtex.2009.00224>. ISSN 1441–8142, paper 1.
- Brandmayr, E., Marson, I., Romanelli, F., Panza, G.F., 2011. Lithosphere density model in Italy: no hint for slab pull. *Terra Nova* 23, 292–299.
- Bruno, P.P., Di Fiore, V., Ventura, G., 2000. Seismic study of the “41st Parallel” fault system offshore the Campanian-Latinal continental margin, Italy. *Tectonophysics* 324, 37–55.
- Cammarano, F., Romanowicz, B., 2007. Insights into the nature of the transition zone from physically constrained inversion of long-period seismic data. *PNAS* 104, 9139–9144.
- Cammarano, F., Goes, S., Vacher, P., Giardini, D., 2003. Inferring upper mantle temperatures from seismic velocities. *Physics of the Earth and Planetary Interiors* 139, 197–222.
- Cammarano, F., Romanowicz, B., Stixrude, L., Lithgow-Bertelloni, C., Xu, W., 2009. Inferring the thermochemical structure of the upper mantle from seismic data. *Geophysical Journal International* 179, 1169–1185.
- Caputo, M., Panza, G.F., Postpischl, D., 1970. Deep structure of the Mediterranean basin. *Journal of Geophysical Research* 75, 4919–4923.
- Caputo, M., Panza, G.F., Postpischl, D., 1972. New evidences about the deep structure of the Lipari Arc. *Tectonophysics* 15, 219–231.
- Carminati, E., Negro, A.M., Valera, J.L., Doglioni, C., 2005. Subduction-related intermediate-depth and deep seismicity in Italy: insights from thermal and rheological modelling. *Physics of the Earth and Planetary Interiors* 149, 65–79.
-   erm  k, V., Kr  l, M., Kre  l, M., Kub  k, J.,   afanda, J., 1991. Heat flow, regional geophysics and lithosphere structure in Czechoslovakia and adjacent part of Central Europe. In:   erm  k, V., Rybach, L. (Eds.), *Terrestrial Heat Flow and Lithosphere Structure*. Springer-Verlag, Berlin, pp. 133–165.
- Conticelli, S., 1998. The effect of crustal contamination on ultrapotassic magmas with lamproitic affinity: mineralogical, geochemical and isotope data from the Torre Alfina lavas and xenoliths, Central Italy. *Chemical Geology* 149, 51–81.
- Conticelli, S., Peccerillo, A., 1990. Petrological significance of high-pressure ultramafic xenoliths from ultrapotassic rocks of Central Italy. *Lithos* 24, 305–322.
- Della Vedova, B., Bellani, S., Pellis, G., Squarci, P., 2001. Deep temperatures and surface heat flow distribution. In: Vai, G.B., Martini, I.P. (Eds.), *Anatomy of an Orogen: The Apennines and Adjacent Mediterranean Basins*. Kluwer Acad. Publ., Dordrecht, pp. 65–76.
- Doglioni, C., 1991. A proposal of kinematic modelling for west-dipping subductions – possible applications to the Tyrrhenian–Apennines system. *Terra Nova* 3, 423–434.
- Doglioni, C., Gueguen, E., Harabaglia, P., Mongelli, F., 1999. On the origin of west-directed subduction zones and application to the Western Mediterranean. In: B. Durand, L. Jolivet, F. Horv  th, M. S  rane (editors), *The Mediterranean Basins: Tertiary Extension within the Alpine Orogen*. Geological Society of London 156, 541–561.
- Downes, H., Kostoula, T., Jones, A., Beard, A., Thirlwall, M., Bodinier, J.-L., 2002. Geochemistry and Sr–Nd isotopic compositions of mantle xenoliths from the Monte Vulture carbonate–mellilitite volcano, central southern Italy. *Contributions to Mineralogy and Petrology* 144, 78–92.
- Frezzotti, M.L., Peccerillo, A., Panza, G.F., 2009. Carbonate metasomatism and CO₂ lithosphere–asthenosphere degassing beneath the Western Mediterranean: an integrated model arising from petrological and geophysical data. *Chemical Geology* 262, 108–120.
- Furlong, K.P., Spakman, W., Wortel, M.J.R., 1995. Thermal structure of the continental lithosphere: constraints from seismic tomography. *Tectonophysics* 244, 107–117.
- Goes, S., Govers, R., Vacher, P., 2000. Shallow mantle temperatures under Europe from P and S wave tomography. *Journal of Geophysical Research* 105 (B5), 11153–11169.
- Green, D.H., Hibberson, W.O., Kov  cs, I., Rosenthal, A., 2010. Water and its influence on the lithosphere–asthenosphere boundary. *Nature* 467, 448–451.
- Hacker, B.R., Abers, G.A., Peacock, S.M., 2003. Subduction factory. 1. Theoretical mineralogy, densities, seismic wave speeds, and H₂O contents. *Journal of Geophysical Research* 108 (B1), 2029, <http://dx.doi.org/10.1029/2001JB001127>.
- Hartmann, G., Wedepohl, K.H., 1993. The composition of peridotite tectonites from the Ivrea Complex, northern Italy: residues from melt extraction. *Geochimica et Cosmochimica Acta* 57, 1761–1782.
- Hauri, E.H., Gaetani, G.A., Green, T.H., 2006. Partitioning of water during melting of the Earth's upper mantle at H₂O-undersaturated conditions. *Earth and Planetary Science Letters* 248, 715–734.
- Hirschmann, M.M., Aubaud, C., Withers, A.C., 2005. Storage capacity of H₂O in nominally anhydrous minerals in the upper mantle. *Earth and Planetary Science Letters* 236, 167–181.
- Hirschmann, M.M., Tenner, T.J., Aubaud, C., Withers, A.C., 2009. Dehydration melting of nominally anhydrous mantle: the primacy of partitioning. *Physics of the Earth and Planetary Interiors* 176, 54–68.
- Jackson, I., 2000. Laboratory measurement of seismic wave dispersion and attenuation: recent progress. *Geophysical Monograph* 117, 265–289.
- Jackson, I., Paterson, M.S., Fitz Gerald, J.D., 1992. Seismic wave dispersion and attenuation in   heim dunite: an experimental study. *Geophysical Journal International* 108, 517–534.
- Jaupart, C., Mareschal, J.-C., 2007. Heat flow and thermal structure of the lithosphere. In: Schubert, G., Watts, A.B. (Eds.), *Treatise on Geophysics*, vol. 6. Elsevier, Amsterdam, pp. 217–252.
- Jessop, A.M., Hobart, M.A., Sclater, J.G., 1976. The world heat flow data collection 1975. *Geotherm Ser.*, 5. Geothermal services of Canada. 125 pp.
- Ji, S., Wang, Q., Salisbury, M.H., 2009. Composition and tectonic evolution of the Chinese continental crust constrained by Poisson's ratio. *Tectonophysics* 463, 15–30.
- Jones, A.P., Kostoula, T., Stoppa, F., Wolley, A.R., 2000. Petrography and mineral chemistry of mantle xenoliths in a carbonate-rich mellilitite tuff from Vulture volcano, Southern Italy. *Mineralogical Magazine* 64, 593–613.
- Karato, S., 1993. Importance of anelasticity in the interpretation of seismic tomography. *Geophysical Research Letters* 20, 1623–1626.
- Karato, S., Jung, H., 1998. Water, partial melting and the origin of the seismic low velocity and high attenuation zone in the upper mantle. *Earth and Planetary Science Letters* 157, 193–207.
- Katz, R.F., Spiegelman, M., Langmuir, C.H., 2003. A new parameterization of hydrous mantle melting. *Geochemistry, Geophysics, Geosystems* 4 (9), <http://dx.doi.org/10.1029/2002GC000433>.
- Kelley, K.A., Plank, T., Grove, T.L., Stolper, E.M., Newman, S., Hauri, E., 2006. Mantle melting as a function of water content beneath back-arc basins. *Journal of Geophysical Research* 111, B09208, <http://dx.doi.org/10.1029/2005JB003732>.
- Kopylova, M.G., Lo, J., Christensen, N.I., 2004. Petrological constraints on seismic properties of the Slave upper mantle (Northern Canada). *Lithos* 77, 493–510.
- Kuskov, O.L., Kronrod, V.A., Annersten, H., 2006. Inferring upper-mantle temperatures from seismic and geochemical constraints: implications for Kaapvaal craton. *Earth and Planetary Science Letters* 244, 133–154.
- Lachenbruch, A.H., 1970. Crustal temperature and heat production: implications of the linear heat-flow relation. *Journal of Geophysical Research* 75, 3291–3300.
- Levshin, A.L., Yang, X., Barmin, M.P., Ritzwoller, M.H., 2010. Midperiod Rayleigh wave attenuation model for Asia. *Geochemistry, Geophysics, Geosystems* 11, Q08017, <http://dx.doi.org/10.1029/2010GC003164>.
- Luth, R.W., 1997. Experimental study of the system phlogopite–diopside from 3.5 to 17 GPa. *American Mineralogist* 82, 1198–1209.
- Mavko, G.M., 1980. Velocity and attenuation in partially molten rocks. *Journal of Geophysical Research* 85, 5173–5189.
- McKenzie, D., Bickle, M.J., 1988. The volume and composition of melt generated by extension of the lithosphere. *Journal of Petrology* 29, 625–679.
- Minster, J.B., Anderson, D.L., 1981. A model of dislocation – controlled rheology for the mantle. *Philosophical transactions of the Royal Society of London* 299, 319–356.
- Morten, L., Bondi, M., 1981. Spinel lherzolite inclusions in basalts from Monti Lessini, Veneto Region, northern Italy. *Neues Jahrbuch fur Mineralogie, Monatshefte* 7, 308–316.
- Nakajima, J., Hasegawa, A., 2003. Estimation of thermal structure in the mantle wedge of northeastern Japan from seismic attenuation data. *Geophysical Research Letters* 30 (14), 1760, <http://dx.doi.org/10.1029/2003GL017185>.
- Panza, G.F., Calcagnile, G., 1979. The upper mantle structure in Balearic and Tyrrhenian bathyal plains and the Messinian salinity crisis. *Palaeogeography, Palaeoclimatology, Palaeoecology* 29, 3–14.
- Panza, G.F., Raykova, R.B., 2008. Structure and rheology of lithosphere in Italy and surrounding. *Terra Nova* 20, 194–199.
- Panza, G.F., Peccerillo, A., Aoudia, A., Farina, B., 2007a. Geophysical and petrological modelling of the structure and composition of the crust and upper mantle in complex geodynamic settings: the Tyrrhenian Sea and surroundings. *Earth-Science Reviews* 80, 1–46.
- Panza, G.F., Raykova, R.B., Carminati, E., Doglioni, C., 2007b. Upper mantle flow in the Western Mediterranean. *Earth and Planetary Science Letters* 257, 200–214.

- Pasquale, V., Verdoya, M., Chirozzi, P., 1996. Some geophysical constraints to dynamic processes in the Southwestern Mediterranean. *Annali di Geofisica* XXXIX (6), 1185–1200.
- Pauselli, C., Massimiliano, R.B., Frederico, C., Magnani, M.B., Minelli, G., 2006. The crustal structure of the Northern Apennines (Central Italy): an insight by the CROP03 seismic line. *American Journal of Science* 306, 428–450. <http://dx.doi.org/10.2475/06.2006.02>.
- Pavese, A., Levy, D., Curetti, N., Diella, V., Fumagalli, P., Sani, A., 2003. Equation of state and compressibility of phlogopite by in-situ high-pressure X-ray powder diffraction. *European Journal of Mineralogy* 15, 455–463.
- Peccerillo, A., 1990. On the origin of Italian potassic magmas: comments. *Chemical Geology* 85, 183–196.
- Peccerillo, A., 2001. Geochemical similarities between the Vesuvius, Phlegraean Fields and Stromboli volcanoes: petrogenetic, geodynamic and volcanological implications. *Mineralogy and Petrology* 73, 93–105.
- Peccerillo, A., 2005. Plio-Quaternary volcanism in Italy. *Petrology, Geochemistry, Geodynamics*. Springer, Heidelberg, 365 pp.
- Peccerillo, A., Lustrino, M., 2005. Compositional variations of the Plio-Quaternary magmatism in the circum-Tyrrhenian area: deep- vs. shallow-mantle processes. *Papers 388 In: Foulger, G.R., Nathland, G.H., Presnall, D.C., Anderson, D.L. (Eds.), Plates, plumes, and paradigms. : Geol. Soc. Am. Spec. Boulder, Colorado*, pp. 421–434.
- Pera, E., Mainprice, D., Burlini, L., 2003. Anisotropic seismic properties of the upper mantle beneath the Torre Alfina area (Northern Apennines, Central Italy). *Tectonophysics* 370, 11–30.
- Phan, H.T., 2008. Elastic properties of hydrous phases in the deep mantle: high-pressure ultrasonic wave velocity measurements on clinohumite and phase A. Ph.D. Thesis, Swiss Federal Institute of Technology, Zürich, Switzerland.
- Priestley, K., McKenzie, D., 2006. The thermal structure of the lithosphere from shear wave velocities. *Earth and Planetary Science Letters* 244, 285–301.
- Riguzzi, F., Panza, G.F., Varga, P., Doglioni, C., 2010. Can Earth's rotation and tidal despinning drive plate tectonics? *Tectonophysics* 484, 60–73.
- Röhm, A.H.E., Snieder, R., Goes, S., Trampert, J., 2000. Thermal structure of continental upper mantle inferred from S-wave velocity and surface flow. *Earth and Planetary Science Letters* 181, 395–407.
- Rosatelli, G., Wall, F., Stoppa, F., Rotolo, M., 2007. Calcio-carbonate melts and metasomatism in the mantle beneath Mt. Vulture (Southern Italy). *Lithos* 99, 229–248.
- Royden, L.H., Burchfiel, B.C., 1989. Are systematic variations in thrust belt style related to plate boundary process? (the western Alps versus the Carpathians). *Tectonics* 8, 51–61. <http://dx.doi.org/10.1029/TC008i001p00051>.
- Sapienza, G., Scribano, V., 2000. Distribution and representative whole-rock chemistry of deep-seated xenoliths from Iblean Plateau, South-Eastern Sicily, Italy. *Periodico di Mineralogia* 69, 185–204.
- Sapienza, G., Hilton, D.R., Scribano, V., 2005. Helium isotopes in peridotite mineral phases from Hyblean Plateau (southeastern Sicily, Italy). *Chemical Geology* 219, 115–129.
- Sartori, R., 2003. The Thyrrhenian backarc basin and subduction of the Ionian lithosphere. *Episodes* 26, 217–221.
- Sassi, F.P., Guidotti, C.V., Rieder, M., De Pieri, R., 1994. On the occurrence of metamorphic 2M1 phengites: some thoughts on polytypism and crystallization conditions of 3T phengites. *European Journal of Mineralogy* 6, 151–160.
- Sato, H., Sacks, S.I., Murase, T., 1989. The use of laboratory velocity data for estimating temperature and partial melt fraction in the low-velocity zone: comparison with heat flow and electrical conductivity studies. *Journal of Geophysical Research* 94, 5689–5704.
- Schmeling, H., 1985. Numerical models on the influence of partial melt on elastic, anelastic and electric properties of rocks. Part I: elasticity and anelasticity. *Physics of the Earth and Planetary Interiors* 41, 34–57.
- Slater, J.G., Jaupart, C., Galson, D., 1980. The heat flow through oceanic and continental crust and the heat loss of the Earth. *Reviews of Geophysics and Space Physics* 18 (1), 269–311.
- Scrocca, D., Doglioni, C., Innocenti, F., Manetti, P., Mazzotti, A., Bertelli, L., Burbi, L., D'Offizi, S., 2003. *Crop Atlas: Deep Seismic Reflection Profiles in Italy: Memorie Descrittive della Carta Geologica d'Italia*, 62. 194 pp.
- Shapiro, N.M., Ritzwoller, M.H., 2004. Thermodynamic constraints on seismic inversions. *Geophysical Journal International* 157, 1175–1188.
- Siena, F., Coltorti, M., 1989. Lithospheric mantle evolution: evidences from ultramafic xenoliths in the Lessinian volcanics (Northern Italy). *Chemical Geology* 77, 347–364.
- Sobolev, S.V., Zeyen, H., Stoll, G., Werling, F., Altherr, R., Fuchs, K., 1996. Upper mantle temperatures from teleseismic tomography of French Massif Central, including effects of composition, mineral reactions, anharmonicity, anelasticity and partial melt. *Earth and Planetary Science Letters* 139, 147–163.
- Sudo, A., Tatsumi, Y., 1990. Phlogopite and K-amphibole in the upper mantle: implication for magma genesis in subduction zones. *Geophysical Research Letters* 17, 29–32.
- Tesauro, M., Kaban, M.K., Cloetingh, S.A.P.L., 2009. A new thermal and rheological model of the European lithosphere. *Tectonophysics* 476, 478–495.
- Toksöz, M.N., Bird, P., 1977. Modelling of temperatures in continental convergence zones. *Tectonophysics* 41, 181–193.
- Tsumura, N., Matsumoto, S., Horiuchi, S., Hasegawa, A., 2000. Three-dimensional attenuation structure beneath the northeastern Japan arc estimated from spectra of small earthquakes. *Tectonophysics* 319 (4), 241–260.
- Wendlandt, R.F., Eggler, D.H., 1980. The origins of potassic magmas: II. Stability of phlogopite in natural spinel lherzolite and in the system $KAlSiO_4$ -MgO-SiO₂-H₂O-CO₂ at high pressures and high temperatures. *American Journal of Science* 280, 421–458.
- Wessel, P.A., Smith, W.H., 1995. New version of the generic mapping tools. Released supplement, *Eos (Transactions, American Geophysical Union)* vol. 76. <http://dx.doi.org/10.1029/95EO00198> 329 pp. www.mantleplumes.org/BananaDoughnuts.html.
- Wyllie, P.J., Sekine, T., 1982. The formation of mantle phlogopite in subduction zone hybridization. *Contributions to Mineralogy and Petrology* 79, 375–380.
- Zanetti, A., Mazzucchelli, M., Rivalenti, G., Vannucci, R., 1999. The Finero phlogopite-peridotite massif: an example of subduction-related metasomatism. *Contributions to Mineralogy and Petrology* 134, 107–122.
- Zappone, A., 1994. Calculated and observed seismic behaviour of the exposed upper mantle. *Surveys in Geophysics* 15, 619–642.
- Zhu, W., Gaetani, G.A., Fusseis, F., Montési, L.G.J., De Carlo, F., 2011. Microtomography of partially molten rocks: three-dimensional melt distribution in mantle peridotite. *Science* 332, 88–91. <http://dx.doi.org/10.1126/science.1202221>.